

# Modeling and investigation of elastomeric properties in materials for additive manufacturing of mechanistic parts

---

Gaurav Goenka

(B. Eng)

A THESIS SUBMITTED

FOR THE DEGREE OF MASTER OF ENGINEERING

DEPARTMENT OF MECHANICAL ENGINEERING

NATIONAL UNIVERSITY OF SINGAPORE

2011

## Acknowledgements

I would like to sincerely thank my supervisor, Associate Professor Ian Gibson for his valuable guidance and support throughout the course of this work. He allowed me enough rope to go out and explore while helping me tie up the loose ends just in time. This work would not have been possible without his remarkable ability to put things into perspective and look at the bigger picture.

I would also like to express my gratitude to Prof R. Narasimhan for his inspirational passion and commitment to problem-solving and research. I am also very thankful to Dr. Nikhil Bhat for helping me get everything together.

Thanks to Mr Low Chee Wah from the Impact Mechanics Lab and Mr Tan Choon Huat from the Advanced Manufacturing Lab for assisting me in the experimental set-up and conducting the experiments. Prof Christopher Yap has been a mentor to me over the past few years and I am extremely grateful to him for his selfless help and support.

Most importantly, I am grateful to my parents and my entire family for their love and encouragement which kept me going through the research. I also thank all my friends and lab-mates for providing me with the much needed breaks from work. I apologize to all those who helped me over the past year whom I have not been able to acknowledge due to space constraints.

## Table of Contents

Acknowledgements.....	i
Summary.....	v
List of Tables .....	vii
List of Figures .....	viii
List of Symbols .....	xi
Chapter 1. Introduction .....	1
Chapter 2. Background .....	6
2.1 Evolution of AM .....	7
2.2 AM Processes .....	10
2.2.1 Stereolithography.....	10
2.2.2 Laser sintering of powders .....	11
2.2.3 Fused Deposition Modelling .....	13
2.2.4 3D Printing .....	14
2.2.5 Jetting.....	15
2.3 Motivation for research .....	19
2.3.1 Important projects in the field .....	22
2.3.2 Scope of present study .....	30
Chapter 3. Theoretical Analysis.....	32
3.1 Initial Theoretical Model.....	33

3.2 Theoretical Living Hinge Model.....	37
3.2.1 Elastic Bending.....	39
3.2.2 Plastic Bending.....	40
3.2.3 Minimum Hinge Thickness.....	40
3.3 Theoretical Modeling of Fullcure720.....	41
Chapter 4. Experimental Study of Material Properties.....	44
4.1 Specimen Fabrication.....	46
4.1.1 Compression Specimen.....	47
4.1.2 Uniaxial tension specimen.....	48
4.2 Testing Procedure.....	49
4.2.1 Compression test.....	50
4.2.2 Tensile test.....	50
4.3 Results and Discussion.....	51
4.3.1 Compression tests.....	51
4.3.2 Tensile tests.....	53
Chapter 5. Numerical Analysis.....	55
5.1 Initial models.....	61
5.1.1 Elastic model.....	61
5.1.2 Plastic-Elastic model.....	64
Chapter 6. Experimental Set-Up.....	70
Chapter 7. Refined Numerical Analysis.....	75

7.2 Refinement of Boundary Conditions .....	75
7.2 2D Model .....	77
Chapter 8. Experimental verification and application of the numerical model .....	80
8.1 Experimental Results .....	80
8.2 Comparison of Experimental and Numerical results.....	82
8.3 Application of Numerical Model – Snap Fits.....	84
Chapter 9. Conclusion.....	91
Bibliography .....	94
Appendix A – Comparison of AM materials for $M_1$ and $M_2$ .....	100
Appendix B – Living hinge specimen dimensions .....	102
Appendix C – Living hinge experimental results .....	104

## Summary

The absence of a design support system providing feature-specific information about Additive Manufacturing (AM) processes and materials has impeded the global acceptance of AM. AM offers designers more geometric complexity than ever before but as we start to use it to build mechanistic parts, we need to replace the conventional process constraints such as draft angles with new process constraints specific to AM to help the designers who want to use the new technology.

This project was initially an investigation into the viability of various AM processes and materials for the fabrication of interlinking structures like living hinges. The initial study focused on the mechanistic properties required for interlinking structures thereby classifying them into material related properties and design-process related properties. A theoretical model was developed to aid material and process selection for living hinges through a study of the elastomeric properties of AM materials and the kinematics of the bending mechanism. The initial analysis led to the hypothesis that it was possible to develop a set of quantifiable rules for living hinges that would allow designers to select the correct process and material from what is available. It predicted that the Objet material FullCure 720 would be a good candidate for the fabrication of living hinges. However, preliminary experimental results and a more detailed theoretical study proved otherwise. While FullCure 720 does exhibit elastomeric properties, it is not strong enough to withstand heavy use.

As a result, the initial hypothesis led to a modified one that it was possible to develop numerical models using Finite-Element Analysis (FEA) which would be able to predict feature behavior. Experiments were carried out to find out the exact material properties of specimens of FullCure 720 fabricated with Objet Eden 350. The results of the experiments were useful to select the most accurate FEA model to simulate the behavior of FullCure 720. After studying and trying numerous plasticity models, the original linear Drucker Prager (DP) model was used in conjunction to the linear elastic model to model the behavior of FullCure 720. A detailed understanding of the living hinge concept as well as elastomeric properties was developed and the FE models were validated with experimental results. The numerical model was subsequently used to simulate the functioning of another mechanism which uses elastomeric properties for its functioning: snap fit mechanisms. The numerical results were in-line with expectations proving that the model could be used to understand the functioning of different mechanisms that use elastomeric properties and could be fabricated using FullCure 720.

## List of Tables

Table 3.1: Material properties of FullCure720 .....	45
Table 4.1: Dimensions for determining compressive properties of specimens .....	51
Table 4.2: Principal theoretical dimensions of tensile specimens .....	52
Table 4.3: Dimensions for determining compressive properties of specimens .....	53
Table 8.1: Dimensions of snap fit .....	90



## List of Figures

Figure 2.1: Evolution of AM (Source: Bourell, 2009).....	9
Figure 2.2: SLA Process .....	12
Figure 2.3: SLA Examples.....	13
Figure 2.4: How the laser sintering of powders works .....	14
Figure 2.5: 3D Printing Examples .....	16
Figure 2.6: The Objet PolyJet process .....	18
Figure 2.7: FullCure 720 enables visibility of internal details (Source: Objet) .....	19
Figure 2.8: TangoBlack offers high flexibility (Source: Objet) .....	19
Figure 2.9: Vase prototype (Source: Objet).....	20
Figure 2.10: Spine prototype (Source: Objet) .....	20
Figure 2.11: AM feature samples (Courtesy EOS and Shapeways) .....	23
Figure 2.12: Comparison between conventional manufacturing and AM.....	24
Figure 2.13: Assessment page from RMSelect.....	27
Figure 2.14: Build time and Cost comparison by RMSelect .....	28
Figure 2.15: Isometric view of a fuel injection system.....	30
Figure 2.16: Sectional view of laser sintered part.....	30
Figure 2.17: Specimen for testing laser sintering .....	32
Figure 2.18: Minimum wall thickness .....	32
Figure 3.1: Selection parameters.....	37
Figure 3.2: Comparison of AM Materials.....	40
Figure 3.3: Principal dimensions of the living hinge.....	42
Figure 3.4: Theoretical model of FullCure720 .....	46
Figure 4.1: Eden 350 (Source: Objet) .....	48

Figure 4.2: Water pressure apparatus for removing support structures .....	49
Figure 4.3: Objet Studio.....	50
Figure 4.4: Shape of test specimen for tensile testing .....	52
Figure 4.5: Photograph of actual specimen.....	53
Figure 4.6: Compression test .....	54
Figure 4.7: Tensile test.....	55
Figure 4.8: Compressive engineering stress vs strain curve .....	56
Figure 4.9: True stress vs logarithmic strain.....	57
Figure 4.10: Tensile engineering stress vs strain curve .....	58
Figure 5.1: Drucker Pragar yield function .....	62
Figure 5.2: Modeling on Solidworks .....	64
Figure 5.3: Screenshot of the elastic model .....	66
Figure 5.4: Element type C3D8R.....	66
Figure 5.5: Hourglass formation .....	67
Figure 5.6: Approximation of the stress vs strain curve .....	69
Figure 5.7: Ramped pressure on the living hinge .....	70
Figure 5.8: Displacement Control Boundary Condition .....	71
Figure 5.9: Semi-circular path traced by node.....	72
Figure 5.10: Path by mid-point of elastic model vs path by semi-circular equations..	73
Figure 5.11: Functioning living hinge model .....	73
Figure 6.1: Living hinge specimen .....	74
Figure 6.2: L-jig to bend the living hinge specimen in a radial path .....	75
Figure 6.3: Clamp to hold specimen from one end during bending .....	76
Figure 6.4: Drawing of the jig to bend the hinge in a vertical path .....	77
Figure 6.5: Experimental set-up with a tensile micro-testing machine .....	77

Figure 6.6: Clamp and specimen .....	78
Figure 6.7: 45 degrees bending achieved using the tensile micro-tester .....	78
Figure 7.1: Boundary conditions during the experiment .....	80
Figure 7.2: Boundary conditions in the FE model.....	80
Figure 7.3: Screenshot of the refined FE model .....	80
Figure 7.4: CFN vs Displacement from refined 3D model.....	81
Figure 8.1: Force vs displacement for varying thicknesses.....	85
Figure 8.2: Force vs Angle of bend for varying thicknesses .....	85
Figure 8.3: Experimental vs numerical results at varying displacements (0.37 mm)..	86
Figure 8.4: Experimental vs numerical results at varying angles of bend (0.37 mm).	87
Figure 8.5: Experimental vs numerical results at varying displacements (0.70 mm)..	87
Figure 8.6: Experimental vs numerical results at varying angles of bend (0.70 mm).	88
Figure 8.7: Bottle cap (example of an annular snap fit) .....	85
Figure 8.8: Box (example of cantilever snap fit) .....	89
Figure 8.9: Cantilever snap fit .....	90
Figure 8.10: Initial position of the snap fit .....	91
Figure 8.11: Snap fit during deflection .....	92
Figure 8.12: Snap fit after passing through ledge .....	93
Figure 8.13: Force required to deflect the beam .....	93
Figure 8.14: Strain on the beam during one cycle .....	94

## List of Symbols

$\varepsilon$ : Elastic strain

$\sigma$ : Elastic stress

$\sigma_f$ : Stress at failure

$\varepsilon_{ultimate}$ : Strain at failure

$M_1$ : Material index 1

$M_2$ : Material index 2

$L_1$  = length of the neutral axis of the living hinge

$L_0$  = length of the outer lower fiber of the hinge

$R$  = hinge radius

$t$  = half of the hinge thickness

$l$  = recess depth

$\theta$ : Bending angle

$(\sigma_1 + \sigma_2 + \sigma_3)$  : Principal stress values

$J_2$  and  $J_3$ : Second and third invariants of the deviatoric part of the Cauchy stress

$\sigma_m$ : Hydrostatic stress.

## Chapter 1. Introduction

Additive Manufacturing (AM) encompasses a range of technologies that are capable of translating virtual solid model data into physical models in a quick and easy process (Gibson et al, 2010). From being used to build crude prototypes with little useful mechanistic properties in the 1980s, AM today has diverse and integral applications in medicine, aeronautics, textiles, etc accounting for almost 1.2 billion USD in 2008 (Bourell et al, 2009).

Various names have been used to describe Additive Manufacturing (AM) in the past. These range from Rapid Prototyping, Rapid Manufacturing, Free-form Fabrication, Direct Digital Manufacturing, and Additive Fabrication to name a few. Each of the names underlines a particular characteristic or virtue of the technology. For example, the name Rapid Prototyping emphasizes on the speed of the technology and its usefulness in making prototypes quickly. Rapid Manufacturing is the use of the technology as part of the total product manufacturing process. Automated Fabrication on the other hand, highlights the automation brought about by the technology while Freeform Fabrication emphasizes on geometry and ability to fabricate complex forms. Layered Manufacturing accentuates the use of layers. Additive Manufacturing underlines the addition of materials during fabrication. In compliance with the recently formed ASTM F42 Technical Committee on Additive Manufacturing, the name Additive Manufacturing (AM) will be used in this paper to refer to a range of technologies that are capable of translating virtual solid model data into physical models in a quick and easy process (Gibson et al, 2010).

In the past few years, improvements in CAD technology combined with the absence of tooling in AM processes has meant that designers no longer need to constrain themselves much by the restrictions of Design for Manufacture (DFM). We are now entering the domain of Manufacture for Design (Hague et al, 2004) where designers can unleash their creativity with relative ease. Better connectivity has led to a greater involvement of the end consumer in the product development process. This has resulted in a greater demand for complex and customized products. At the same time, advancement in AM machine technology has finally allowed users to fabricate products with sufficient accuracy and useful mechanistic properties. With the agreement between HP and Stratasys to build 3D Printers together (Shankland, 2010), AM today may stand on the cusp of realizing its potential and being used in the mainstream manufacturing industry through mass customization. This could amount to a new industrial revolution in 5-10 years (Griffiths, 2005) by changing the paradigm of manufacturing, service and distribution. It would simultaneously provide opportunities for producing highly complex, custom-made products at low cost in or outside the conventional factory, possibly by distributor, retailer or customer (Hague et al, 2003).

Nonetheless, there are a few areas which need to be addressed before AM can truly be accepted as a viable method for manufacturing. The Roadmap for Additive Manufacturing (RAM) workshop held at UT Austin in 2009 articulated how research in AM over the next 10-15 years would accelerate the integration of AM technologies into the marketplace. One of their recommendations was the creation of conceptual design methods to help designers define and explore design spaces enabled by AM and the designing of a support system which would assist them in navigating complex

process-structure-property relationships. Indeed it is true that while it is now possible to include integral gears and cams, mechanical and living hinges, snap fasteners and even fully interlocking meshes such as chain mail within a single manufacturing stage with AM technology, there are currently very few tools that support the design process with focus on AM technologies (Gibson et al, 2010).

Among the notable studies that have tried to address the problem was the ‘Design for Rapid Manufacturing’ project at Loughborough University undertaken by Campbell and Hague (Hague et al, 2004). They investigated how the advent of the technology would affect the design and manufacturing phases of complex plastic components. They focused on developing a database that indicated to the designer the features that could be included in the product while using AM processes based on experiences of previous designers. EOS, a company focusing on the laser sintering of powders also carried out a study proposing a variety of living hinge designs. However both these projects fell short of quantifying the outcomes of the design proposals.

This project was initially an investigation into the viability of various AM processes and materials for the fabrication of interlinking structures such as living hinges. It was an effort to understand the material issues in parts made using AM so that we may be able to develop a set of quantifiable rules that allow designers to exploit them. Designers could use these rules to select the correct process and material from what is available for their particular design feature. It would also serve as a pointer to determine whether a specific design might work once it has been fabricated. Over the course of the project, as a detailed understanding of the living hinge concept and

elastomeric properties was obtained, it was found to have been possible to develop and validate numerical models that were based on the principles of elasticity, plasticity and visco-elasticity.

Chapter 2 of this thesis provides the bedrock of the research work by chronicling the evolution of RP to AM while simultaneously explaining the advantages and disadvantages of the various AM. It goes on to discuss in detail, the different issues which need to be resolved in order to precipitate the integration of AM into mainstream manufacturing. It also discusses the previous work carried out in the area and aims to justify the motivation behind undertaking the research work.

Chapter 3 represents the initial study which focused on the mechanistic properties required for interlinking structures thereby classifying them into material related properties and design-process related properties. It also introduces the preliminary theoretical model developed to aid material and process selection for living hinges through a study of the elastomeric properties of AM materials and the kinematics of the bending mechanism.

Chapter 4 explains the experimental analysis of elastomeric properties with living hinges as an example. The Objet Eden 350 machine which uses the PolyJet Matrix 3D Printing technique was chosen for the study due to availability while FullCure 720 was chosen as the material for the investigation. Results of the various tests carried out are presented and analyzed.



Chapter 5 presents the development of a general Finite Element Analysis (FEA) model taking living hinges as an example which could be used to model different features that make use of the elastomeric properties of FullCure 720 or similar materials. It investigated the high deformation which occurs during the bending of a feature and examined the ability of FEA to predict the feature behavior by obtaining simulation results from a model that undergoes high element distortion.

Chapter 6 explains the experimental set-up that would closely resemble the real life functioning of a living hinge while allowing repeatability and measurability.

Chapter 7 shows the refining of the FE model developed in Chapter 5 to adapt it to boundary conditions described in Chapter 6. Since the feature modeled had a constant geometry throughout the cross-section, a two-dimensional model was also developed in order to reduce the solver time.

Finally Chapter 8 compares the experimental results with the results from the numerical analysis. It also shows an application of the numerical model to simulate the functioning of another mechanism using elastomeric properties, snap fit mechanisms.

## Chapter 2. Background

This section provides an overview of the development of AM processes over the years while analyzing their merits and weaknesses. It goes on to discuss in detail the different issues that need to be resolved in order to precipitate the integration of AM into mainstream manufacturing. It also discusses the previous work carried out in the area and aims to justify the motivation behind undertaking this research.

AM consists of far too many technologies to be described comprehensively within the scope of this work. Indeed, more than 920 AM related patents have been issued in the US alone (Hague et al, 2003). While most of these processes never achieved technical and commercial success and were slowly forgotten, some of the processes like laser sintering of powders, Stereolithography (SLA), Fused Deposition Modeling (FDM) and 3D Printing have become popular in recent years and will be discussed in detail here. While each of the processes has unique characteristics, they are fundamentally all layered manufacturing processes which form 2D cross-sections of finite thickness one on top of the other thus generating 3D forms. They are also fixture-less (some make use support structures during fabrication) and tool-less. The principle difference between the processes lies in how the layers are produced and bonded.

## 2.1 Evolution of AM

The early roots of AM have been identified in topography and photosculpture (Bourell et al, 2009). In topography, the beginning of AM can be traced to 1890 when Blanther proposed a layered method for making a mold to aid topographical relief maps (Blanther, 1892). Figure 2.1 shows the major events which shaped the field in its nascent years.

TOPOGRAPHY		PHOTOSCULPTURE	
Blanther patent filed	1890	1860	Willeme photosculpture
Perera patent filed	1937	1902	Baese patent filed
Zang patent filed	1962	1922	Monteah patent filed
Gaskin patent filed	1971	1933	Morioka patent filed
Matsubara patent filed	1972	1940	Morioka patent filed
DiMatteo patent filed	1974	1951	Munz patent filed
Nakagawa laminated tool fabrication	1979		
		1968	Swainson patent filed
		1972	Ciraud patent filed
		1979	Housholder patent filed
		1981	Kodama patent filed
		1982	Herbert patent filed
		1984	Maruntani patent filed, Masters patent filed, Andre patent filed, Hull patent filed
		1985	Helysis founded, Denken venture started
		1986	Pomerantz patent filed, Feygin patent filed, Deckard patent filed, 3D founded, Light Sculpting started
		1987	Fudim patent filed, Arcella patent filed, Cubital Founded, DTM founded, Dupont Somos venture started
		1988	First shipment by 3D, CMET founded, Stratasys founded
		1989	Crump patent filed, Helsinki patent filed, Marcus patent filed, Sachs patent filed, EOS founded, BPM Tech. founded
		1990	Levant patent filed, Quadrax founded, DMEC founded
		1991	Teijin Seiki venture started, Foeckele & Schwartze founded, Soligen founded, Meiko founded, Mitsui venture started
		1992	Penn patent filed, Quadrax acquired by 3D, Kira venture started, Laser 3D founded, First shipment by DTM
		1994	Sanders Prototyping started
		1995	Aaroflex venture started
		1997	AeroMet formed, Optomec restarted, ZCorp started
		1998	Objet founded, Keicher patent filed
		1999	POM founded, BPM closed
		2000	Helisys closed, Solidica started
		2001	3D and DTM merge

Figure 2.1: Evolution of AM (Source: Bourell, 2009)

Since the late 1980s, AM has seen a colossal increase in the amount of interest and activity displayed in it. Between 1985 and 1990, numerous companies were founded including Helysis, 3D Systems, DTM, Stratasys, CMET, Cubital, EOS, DMEC and Quadrax all with the idea of advancing the technology and commercializing it. Even though some of these companies failed, others such as EOS, 3D Systems and Stratasys still exist. Along the way, important patents were published by Deckard, Crump, Penn and Sachs. The company Z Corp was founded in 1997 while Objet was started in 1998.

Over the past twenty years AM has evolved from being used to make visual prototypes to recently being used in the standard manufacturing process of the Boeing 787 Dreamliner. This has occurred due to several reasons, some of which have been discussed below:

Improvements in part processing: Most of the earlier RP processes required manual post-processing which was time-consuming and deterred the growth of its usage. Most RP processes still require a certain amount of post-processing. However the introduction of techniques such as water soluble supports has meant that their removal is no longer a cumbersome affair. Furthermore, surface treatments have also emerged which provide environmental protection to the part while reducing surface roughness, adding surface hardness and providing a choice of adding color to the part.

Direct metal fabrication: The advent of various commercial processes that allow sintering of powders of steel, titanium, cobalt, chromium, etc has opened a new sphere of AM applications. While grain size and density remain an issue with direct metal fabrication, the process nevertheless, has huge potential.

Polymer material development for functional applications: Improvements in tensile behavior, thermal properties (in particular max temperature), etc in polymers have led to their usage for functional applications such as living hinges, gears and chains to name a few. Polymers forming composites with glass, etc have recently been introduced and look promising.

Requirements for new industrial products: Today there is an ever greater demand for customized goods with low volume requirements, high geometric complexities and fast turnaround which has led to the increased usage of AM increasingly in industry. Industries such as aerospace and bio-mechanics, which require high precision along with high customization and low volume, have been increasingly using AM providing the technology oxygen in the form of financial support and user feedback. Other fields such as designer products, artistic fabrication (Shapeways) and toys for gaming support (FigurePrints) have also started driving the technology forward by bringing it into the limelight.

## 2.2 AM Processes

### 2.2.1 Stereolithography

Stereolithography (SLA), primarily marketed by 3D Systems Inc is a process which builds plastic parts using a focused laser beam to solidify a photosensitive liquid. The part is built by the repeated scanning of successive layers derived from the original CAD file. The photosensitive liquid quickly solidifies wherever the laser beam strikes its surface. Once a layer is completely traced, it is lowered a small distance so that a thin layer of the liquid covers the solid surface which is in-turn solidified using the focused laser beam. The self-adhesive property of the material causes the layers to bond with one another eventually forming a complete 3D object (Yuan, 2008). Figure 2.2 provides a pictorial representation of the SLA process.

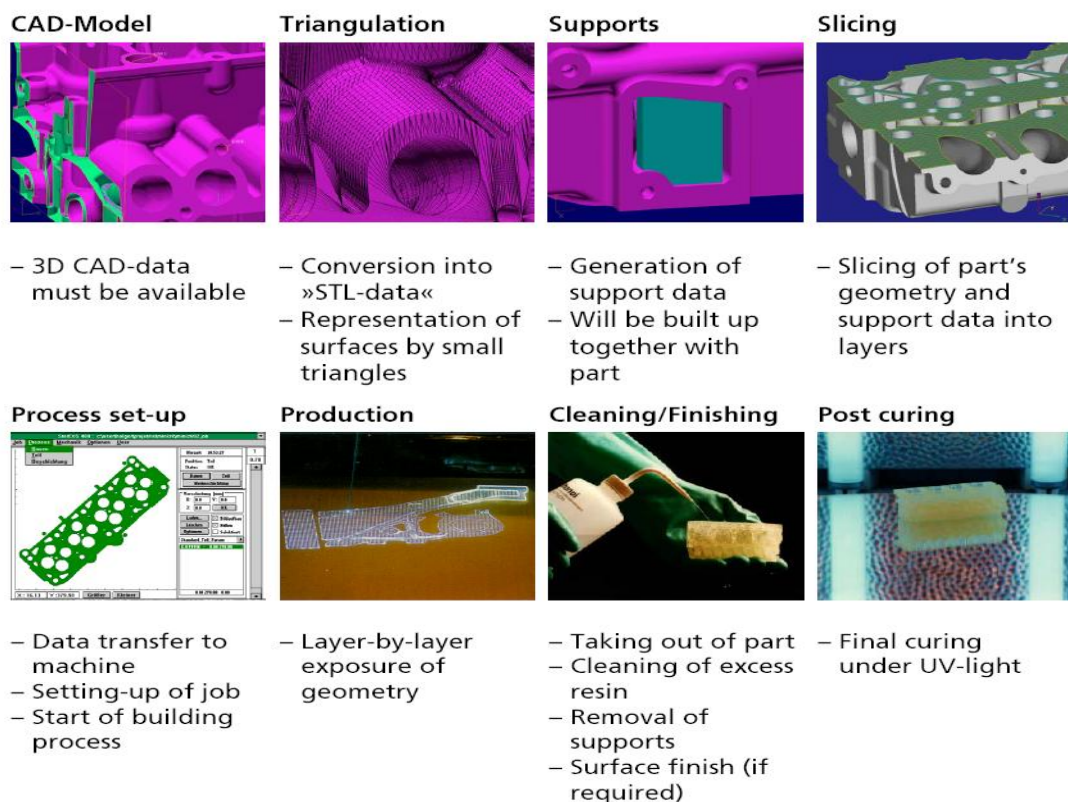


Figure 2.2: SLA Process

The specially designed materials offer mechanical properties very similar to thermoplastics (eg. polypropylene). SLA offers very good tolerances with a layer thickness of 0.025 mm with vertical repeatability of 0.001 mm and a drawing speed of 9.52 m/s. As SLA is a liquid based process, the parts have a good surface finish but there still exists a need for support structures to connect the part to the build platform and support the overhanging features. Also, a post-curing apparatus is required and the material properties of the parts tend to degrade on exposure to sunlight (Gibson et al, 2010). Figure 2.3 shows a few examples of parts made from SLA.



Figure 2.3: SLA Examples

### 2.2.2 Laser sintering of powders

Developed at the University of Texas (Austin), laser sintering of powders uses a high power laser beam such as CO<sub>2</sub> to fuse small powder particles of plastic, metal, ceramic or glass. The powder particles are either melted or are coated with a thermoplastic binder in order to form a solid layer. Once a layer has been formed, loose powders are spread using a roller and the process is repeated till the desired 3D form is achieved. The fabrication chamber is maintained at a temperature just below

the melting point of the powder so that the laser beam only has to elevate the temperature slightly for sintering to occur. Figure 2.4 shows how the process works.

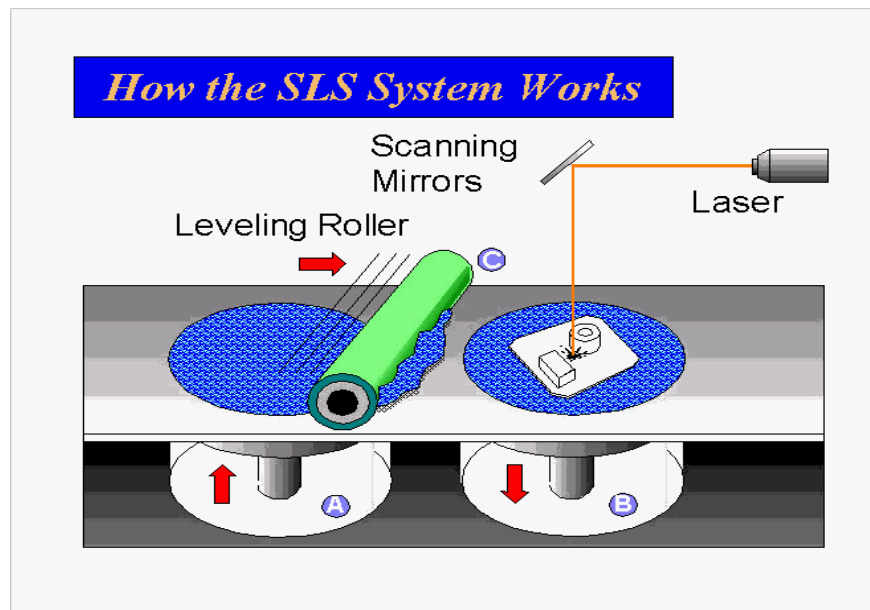


Figure 2.4: How the laser sintering of powders works

Current materials being used in laser sintering of powders include polyvinyl chloride, polyester, ABS, nylon, polycarbonate and investment casting wax. Ceramic and metal powder could also be used for higher powered systems. The process allows high part complexity since it does not require any support structures (the support is provided by the unfused powders). On the other hand, being powder based causes the parts to have high porosity and surface roughness.

Both EOS GmbH and 3D Systems provide machines and materials for laser sintering of powders. The EOS P 760 is able to provide an effective build volume of 700mm x 380 mm x 580 mm with a build speed of up to 32 mm/h. It offers a layer thickness of between 0.06 – 0.18 mm depending on the material. The recently introduced Celerity



Beam Delivery System by 3D Systems allows fast scanning at higher laser power. Other scanning strategies that focus on minimizing the scan time are also being developed. There is increased drawing speed of 10 m/s and improved dimensional accuracy of approximately 20% in x,y and z directions.

### **2.2.3 Fused Deposition Modelling**

Fused Deposition Modelling (FDM) is a process that consists of melting of a wire-shaped plastic material and deposition using an extrusion nozzle. As the nozzle is moved over the table according to the required slice geometry, it deposits a thin bead of extruded plastic to form each layer. The plastic hardens immediately after being projected from the nozzle and bonds with the layer below. The entire system is contained within a chamber where the temperature is held below the melting point of the plastic.

FDM uses thermoplastics such as ABS, Nylon, Wax, etc as building material. It allows for limited part complexity due to the need of support materials which are removed in the end by either breaking them away or washing them away if they are water soluble. The maximum part size is 600 x 500 x 600 mm<sup>3</sup> with an accuracy of 0.1 mm. Recent advances in FDM technology include the MagnaDrive technology with XY electromagnetic motion control system and dual-axis linear motors which hope to improve process speed, accuracy and part complexity.

### 2.2.4 3D Printing

The process, primarily marketed by Z Corp involves local bonding of powder by a binder using an ink jet (patent of MIT). The powdered material could be plastic, ceramic, metal or cermets amongst others. The inkjet layer then ejects bonding material onto successive layers. Like the laser sintering of powders, no support structures are needed because the excess powder on the build piston acts as a support during the build. Once the part is de-powdered, the part can be finished using infiltrates varying from wax, cyanoacrylate and epoxy materials, to increase strength and achieve a desirable finish.

The build speed is very high and easy to handle. Additionally, the binder is available in different colours and can be printed using colour printing techniques to produce full colour parts. The process is ideal for visualization but substandard in terms of mechanical properties. The maximum part size is 200 x 250 x 200 mm<sup>3</sup> with a resolution of 600 dpi in x-y direction. Recent advances include a faster, colour machine from Z Corp called Z406 3D Color which prints up to 160 cubic inches per hour. Figure 2.5 shows a few examples of parts made from 3D Printing.



Figure 2.5: 3D Printing Examples

### 2.2.5 Jetting

Jetting uses ink-jet type processes to fabricate solid objects. Sanders Prototype (now known as Solidscape) was amongst the pioneers of jetting. Founded in 1994, it introduced ModelMaker which uses thermoplastic and wax to build prototypes. The machine uses a jet piezoelectric deposition head to lay down the primary structure. The support structure is laid using a second wax material with a lower melting temperature. The droplets from these print heads are very small so the resulting parts are fine in detail (Gibson et al, 2010). However the Solidscape machines are rarely used in applications other than jewelry and medical devices. Presently the jetting process is primarily marketed by Objet Geometries which launched its first machine in 2000 based on the PolyJet Matrix technology. As shown in Figure 2.8, the jetting head slides back and forth along the X axis depositing a single very thin layer photopolymer onto the build tray (Smiley, 2008). UV bulbs placed alongside the jetting bridge emit UV light immediately after building each layer which leads to their immediate curing and hardening. This eliminates the need for additional post-curing. The internal jetting tray moves down and the jet head prints another layer. This process is repeated till the model is complete. There are eight print heads each containing 96 nozzles which are managed by the process software to work in parallel (Objet, 2010).

Unlike in laser sintering of powders, support materials are required in this process. The support material, which is also a photopolymer but undercured and therefore softer, is removed by washing it away with pressurized water in a secondary operation. While the older Objet Eden machines were only able to print one material

at a time, the newer Connex machines provide multi-material capability. This allows the variation of material properties such as tensile strength, elongation strength, etc. according to the needs of the design.

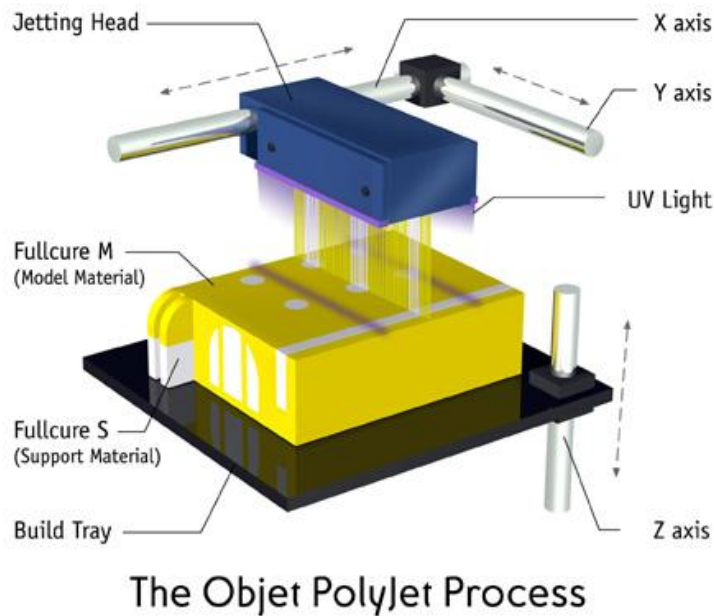


Figure 2.6: The Objet PolyJet process

Objet provides several materials which could be used in the process. For example, FullCure is a translucent, acrylic-based photopolymer material which can be used to make a transparent object. It provides good impact strength and a moderate elongation at break of 20%. It also enables visibility of liquid flow and internal details as shown in Figure 2.7. Vero materials provide opaque surfaces (available in blue, white, gray and black) with good impact strength and flexural strength. Tango materials are rubber-like flexible materials as shown in Figure 2.8 with very high elongation at break (especially for TangoPlus and TangoBlackPlus). The applications include consumer electronics applications, shoes, toys, general industrial applications, and rapid tooling.



Figure 2.7: FullCure 720 enables visibility of internal details (Source: Objet)



Figure 2.8: TangoBlack offers high flexibility (Source: Objet)

The Eden350 has a tray size of 350mmx350mmx200mm with part resolution of  $42\mu$  on the X-axis,  $42\mu$  on the Y-axis and  $16\mu$  on Z-axis. The z-resolution is then translated into jetting a  $16\mu$  layer thickness onto a build tray. This implies that the stair effect on parts is reduced, so there is likely to be less of a need for hand finishing. It also results in smooth surfaces for simple to complex geometries. However, this generally slows down the speed which is approximately 6.5 mm/h and many parts are built with larger layer thicknesses.

As seen in Figures 2.9 and 2.10, the process is capable of producing parts with smooth curves closely resembling the final product. Even though Objet machines provide

specifications similar to SLA, they are cheaper and more convenient thereby making it an important technology to observe.



Figure 2.9: Vase prototype (Source: Objet)



Figure 2.10: Spine prototype (Source: Objet)

## 2.3 Motivation for research

The first AM machines were expensive, inaccurate and slow to build a single part from equally expensive materials. Furthermore, they had poor mechanical properties and suffered from long-term degradation and distortion effects. As a result, it was always assumed that the final product would be made using conventional processes. However, over the past few years, incremental improvements in the technology have focused on lowering machine costs whilst increasing build speeds and accuracies. Parallel improvements in materials have resulted in a wider range of materials with superior properties that are consequently suited to a much wider range of applications. Many of these applications are now destined for final use rather than just the earlier stages of the product development process. For example, Jan Eggert from the Rapid Technology Center (RTC) at BMW explained at the Additive Manufacturing Conference International Conference 2010 at Loughborough University how AM has helped BMW in the development of new products by shortening product development cycles.

It is now possible to include integral gears and cams, mechanical and living hinges, snap fasteners and even fully interlocking meshes such as chain mail into a design and in a single manufacturing stage with AM technology (like the examples shown in Figure 2.11). Metal systems have also become a reality in recent years to enhance this rich arsenal of tools that can tie design to manufacture in such an unprecedented manner.

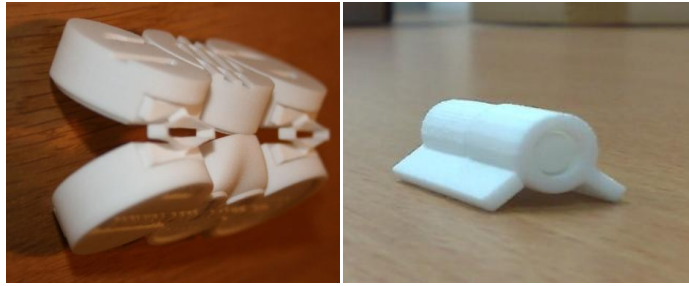


Figure 2.11: AM feature samples (Courtesy EOS and Shapeways)

The possibilities offered by AM today are profound. As shown in Figure 2.12, AM enables the shortening of manufacturing processes by reducing process planning, shortening the production cycle, eliminating the need for extensive tooling or fixturing and simplifying the logistics. This allows us to cope with immediate demand while simultaneously being able to incorporate custom elements into the product even with small batches. AM also enables us to reduce the number of components in the design while being able to combine different materials using processes such as laser sintering of powders and PolyJet Matrix (Objet) in order to form new exotic materials that best suit their needs.

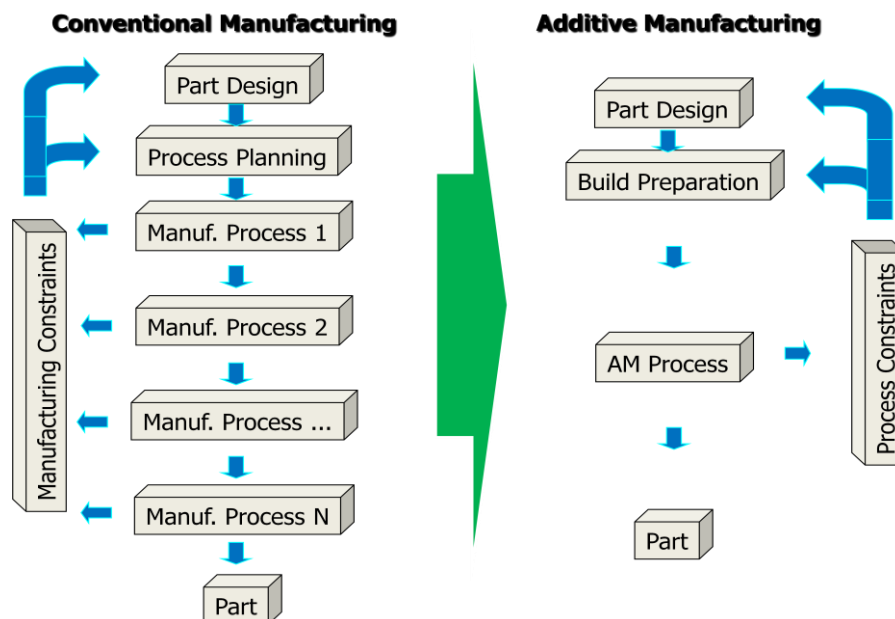


Figure 2.12: Comparison between conventional manufacturing and AM (Source: Pham and Dimov, 2001)



Perhaps the biggest advantage of AM is the ability to manufacture parts of virtually any complexity without the need for tooling. The need for tooling in conventional manufacturing represents one of the most restrictive factors for today's product development (Hague et al, 2004). For example, some guidelines for injection moulding are:

Draft angles: Draft angles are important for the removal of parts from moulds.

Wall-thickness consideration: Thin walls solidify faster, thus reducing warpage and production costs.

Uniform wall thickness: Cracks, crazing and fractures can be caused due to the compressive and tensile stresses subsequently present in the parts due to non-uniform wall thickness.

Minimizing weld lines: When different flow fronts meet each other due to obstruction within the mould or various gates, it causes weld lines which are aesthetically unpleasant and also a source of weakness in the part.

Ejection pin marks and gate marks: They could have a negative aesthetic effect on the part.

Minimizing overhangs and other complex features: Require multiple stage moulds

The freedom of design offered by AM enables designers to 'Manufacture for Design' rather than 'Design for Manufacture'. Unfortunately, the freedom of design offered by AM is still not being fully exploited by designers. Till date, most of the products fabricated using AM are slightly customized versions of designs intended for injection

molding where AM is used to achieve customization for small batches. Designers still do not design products especially for AM processes. One of the main reasons that AM processes are rarely used to produce end-use parts is the lack of data and support available to designers with respect to AM. As we start to use AM to build mechanistic parts, we need to replace the conventional process constraints such as draft angles with new process constraints specific to AM. These constraints are certainly more relaxed in terms of overall functionality of part, but we must still understand the process and materials completely in order to get the best out of the resulting parts and to avoid errors, delays, etc.

The Roadmap for Additive Manufacturing (RAM) workshop (UT Austin, 2009) also recommended the creation of conceptual design methods to help designers in defining and exploring design spaces enabled by AM. According to them, this would help accelerate the integration of AM technologies into the marketplace. Furthermore, they recommended designing a decision support system to assist in navigating complex process-structure-property relationships so that it would encourage more designers to adopt AM. The panel also suggested the creation of methods to model and design with variability: shape, properties, process, etc.

### **2.3.1 Important projects in the field**

The idea of building a database to help designers in AM processing and material selection is not new. Over ten years ago, Rosen at Georgia Tech proposed the development of a decision support system to answer the following questions:

- **Quotation support:** Given a part, what machine and material should I build?
- **Capital investment support:** Given a design and industrial profile, what is the best machine that I can buy to fulfill my requirements?
- **Process planning support:** Given a part and a machine, how do I set it up to work in the most efficient manner alongside my other operations and existing tasks?

Rosen developed a software called RMSelect in 2005 to address the issue. In the software, a 'Project Data' menu asks for information regarding the project including production rate (parts/week), part cost (target), project duration and part life. The 'Part Data' menu asks for part specific information such as size, surface finish, smallest feature size, etc. The 'Qualitative' menu asks multiple-choice questions regarding part complexity, part consolidation and turn-around time for part orders. Based on the above information, the software presents preliminary results displaying the machines that are capable of fabricating the part. The 'Assessment' tab shows details about the build time and cost benefits as shown in Figure 2.13 and 2.14. However, the software failed to advise users on what design changes could be made to ensure that other RP machines could also be used.

Alternatives	Materials	Build Vol.	Surf Fin.	Tolerance	Feature Size	Cost
SLA Viper	Y	Y	Y	Y	Y	1992.71
SLA-5000	Y	Y	Y	Y	Y	1062.05
SinterStn HIQHS	Y	Y	N	Y	Y	188.71
SinterStn Pro140	Y	Y	N	Y	Y	261.78
Targets	Polymer	---	3.000	20.000	1.000	200.00

Figure2.13: Assessment page from RMSelect

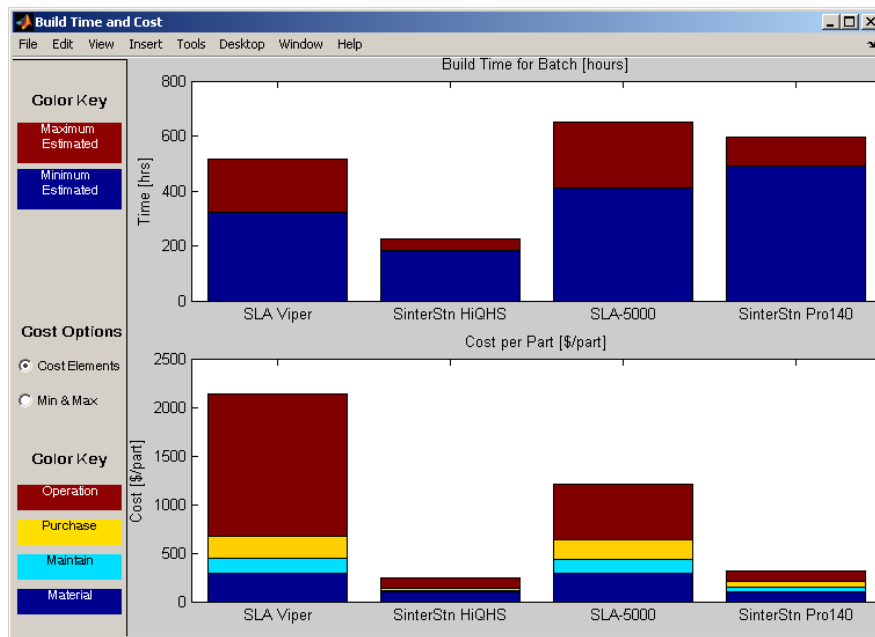


Figure 2.14: Build time and Cost comparison by RMSelect

Recognizing the need for a design support system, the ‘Design for Rapid Manufacturing’ project at Loughborough University, UK was launched with the objective of investigating how the advent of AM would affect the design and manufacturing phases of complex plastic components. It also aimed to characterize

and analyze the material properties of AM materials thus enabling designers to have confidence in specifying the materials for their designs. Hague et al investigated how the advent of Rapid Manufacturing could influence an individual designer's approach to product design and material selection. It was assumed that problems of accuracy, surface finish and repeatability had been resolved. The processes and the materials selected for the project were:

- SLA7000 which uses the SLA process
  - SL7560 by Huntsman
  - SI40 by 3D Systems
- LS Vanguard Si2 which uses the laser sintering process
  - Duraform PA by 3D Systems

These processes and materials were selected due to their conversion potential for future manufacturing systems. Tensile, flexural and Izod impact tests were carried out over temperatures ranging from  $-40^{\circ}$  to  $+40^{\circ}$  C, different humidities (dry, controlled and wet) and over extended times (1,4,13,26 and 52 weeks). Given the layer-wise nature of the manufacturing technique, isotropy tests were also performed because if the materials were isotropic then it would allow the freedom of choosing the build orientation without affecting the mechanical properties of the produced products. In total, around 5500 individual tests were conducted. It was concluded that SLA parts are broadly isotropic with respect to laser sintering parts whose mechanical properties and surface quality are affected by the build orientation. The effect of temperature on UTS and Young's modulus was studied. From this, it was concluded that while SLA parts have higher UTS and stiffness, laser sintering parts maintain their properties over a broader temperature range.

The front component of a fuel injection system assembly as shown in Figure 2.15 was investigated for fabrication using AM. The component which could have an operating temperature of 200° C requires a material which should be able to cope with exposure to water, oil, diesel fuel and salt spray. It has conventionally been fabricated using gravity castings. The produced castings undergo secondary operations to create long holes which are subsequently required to be blanked off. This phase is not only time consuming and expensive but also risky as it allows the possibility of fuel leakage during the working of the injection system. Additionally, non-straight galleries cannot be designed which renders the system unable to allow low-pressure circuit flow.



Figure 2.15: Isometric view of a fuel injection system

The front plate was thus redesigned for AM using both laser sintering and SLA. While the part was easily produced using laser sintering, SLA proved more difficult in this case as it was difficult and time-consuming to remove the support structures inside the galleries. Figure 2.16 shows a sectional view of the laser sintered part.



Figure 2.16: Sectional view of laser sintered part

The study showed that it is possible to eliminate secondary operations needed in conventional manufacturing while reducing the potential for fuel leakage. However, while AM was able to solve the design problem, the study found that current available AM materials did not satisfy the operating temperature range of  $-40^{\circ}$  to  $140^{\circ}$  C and more research is needed to be carried out in the domain.

At Loughborough University, Maidin and Campbell are aiming to develop a knowledge based tool for laser sintering of powders in order to capture the tacit knowledge of professional designers who currently design for RM through a semi-structured interview approach. An initial attempt involved interviewing four experienced designers on AM case study products that exhibited geometric complexity, parts complexity and product customization.

EOS GmbH also undertook a study (Sippel, 2008) to develop a set of design rules aimed at designers wishing to use laser sintering. Materials were tested for accuracy, anisotropy, wall thickness, holes, pins, clearances, tolerances, etc. A specimen (Figure 2.17) was fabricated to test the accuracy of laser sintering for labeling quality in various directions. The side part and the bottom part of the specimen showed very good labeling quality compared to the top part.

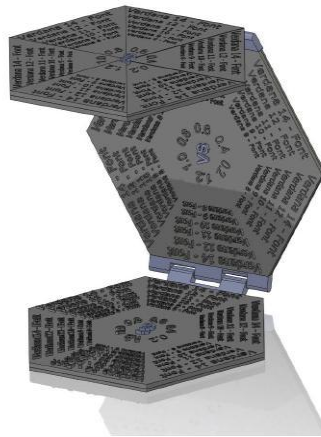


Figure 2.17: Specimen for testing laser sintering

There was a maximum deviation of  $\pm 0.06\text{mm}$  in the wall thickness and the minimum wall thickness of a part was recommended to be 1mm. The minimum achievable hole size was shown to depend on the wall thickness as shown in Figure 2.18.

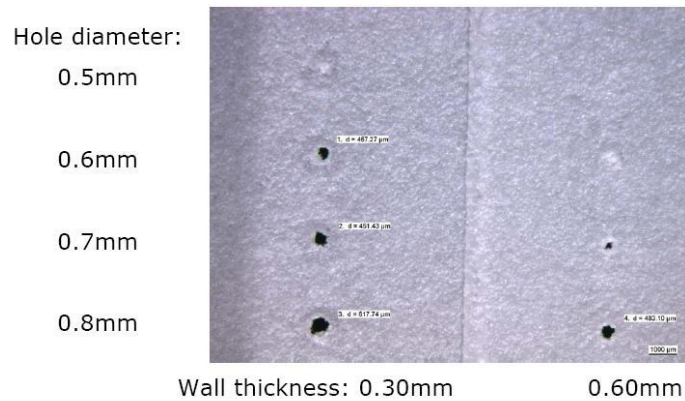


Figure 2.18: Minimum wall thickness



The RMSelect project gave the designer a very good idea of the build time and cost with respect to different processes and materials. It also introduced to the designers new processes and machines potentially capable of fabricating the product which he/she previously might not have been aware of. However, the project remained largely macroscopic in its approach and did not feature specific information to designers. On the other hand, the 'Design for Rapid Manufacture' project at Loughborough investigated various designs including a fuel injection system, an alarm clock, etc but fell short of quantifying the outcomes of any design proposals. Campbell and Choi (Cheug and Choi, 2008) tried to simulate AM technology so that users and designers could understand how parts, for example might be affected by the layer-based technology and the orientation inside the machine. However, this was more analytical and did not provide any initial rules for such a design. The EOS project went one step further by quantifying the capabilities of laser sintering for simple features such as labelling, walls, holes, pins, gaps, etc. They even recommended a set of basic design rules such as minimum hole size, etc. They also carried out a study that proposed a variety of living hinge designs based on a basic set of material properties (Gonzales and Kerf, 2008). This study could help designers understand how different designs might function but it is still somewhat difficult to understand how to fine-tune a design using the proposed hinge designs. Additionally, while they quantified the results regarding the process and material capabilities for simple features such as holes and pins, the study stopped short of quantifying the outcomes regarding mechanistic parts such as living hinges.

Presently, companies such as Shapeways ([www.shapeways.com](http://www.shapeways.com)), Freedom of Creation ([www.freedomofcreation.com](http://www.freedomofcreation.com)) and MGX ([www.materialise.com](http://www.materialise.com)) are at the forefront of providing innovative designs that exploit the capabilities of AM technology. However, these companies are also exploiting their position in the marketplace, having an extensive understanding and experience of the technologies. As a result, there are currently very few tools in the public domain that support the design process with focus on AM technologies.

### **2.3.2 Scope of present study**

The purpose of this study was to try and understand the material issues in parts made using AM so that we may be able to generate a set of quantifiable rules that can allow designers to exploit them. There are numerous AM technologies available, with new processes and machines being introduced to the market at regular intervals. Existing machines are also extended by the introduction of new materials and innovative post-processing techniques. It is therefore important to focus on design rules that are flexible enough to accommodate these technological developments. By doing so, we can: -

- Choose the correct process and materials from what is available.
- Define lower limits that can ensure a design feature will probably work for the chosen machine parameters.
- Determine whether a specified design might work once it has been fabricated.

At the outset, this project was an investigation into the viability of various AM processes and materials for the fabrication of interlinking structures such as living hinges. Initial analysis led to the hypothesis that it was possible to develop a set of quantifiable rules for living hinges that would allow designers to select the correct process and material from what was available. Preliminary experimental results and a more detailed theoretical study proved otherwise. As a result, the initial hypothesis led to a modified one that it was possible to develop numerical models with the help of Finite-Element Analysis (FEA) that would be able to predict feature behavior. Over the course of the project, a detailed understanding of the living hinge concept as well as elastomeric properties was developed and the Finite Element models were validated with experimental results.

## Chapter 3. Theoretical Analysis

The objective of this part of the research work was to understand the underlying physics of the movement of interlinking structures. It starts with a study of different mechanistic properties required for interlinking structures classifying them into material and design-process related properties. It describes a preliminary theoretical model developed through the study of the elastomeric properties of AM materials and the kinematics of the bending mechanism. This is followed by a more sophisticated theoretical model based on beam theory.

There are numerous mechanistic properties which influence the functioning of a part/feature and also the overall cost of the part/feature. As a result, these are used in material and process selection. Mechanistic properties can be classified into material related properties and process related properties. Material related properties can be further classified into intrinsic material properties which include density, strength, stiffness, hardness, thermal conductivity, electrical conductivity, elastic storage capacity, porosity, permeability, chemical reactivity, coefficient of friction and corrosion resistance. The external properties affect material selection even though they do not affect feature performance. They include cost, availability and aesthetics.

The design of the part also affects the material and process selection. For example, it is difficult to fabricate mechanical hinges using SLA since it requires support structures which might be difficult to remove once the part has been completed. On the other hand, the feature can be built using laser sintering but the clearances should

be big enough for the powder particles to be able to come out of the hinge. The speed of the process is another criterion as some parts have a high turn-around time. Part finishing is extremely important as it affects the surface smoothness, coloration, hardness, tensile properties, UV protection as well general aesthetics of the part.

Figure 3.1 shows a summary of the selection parameters:

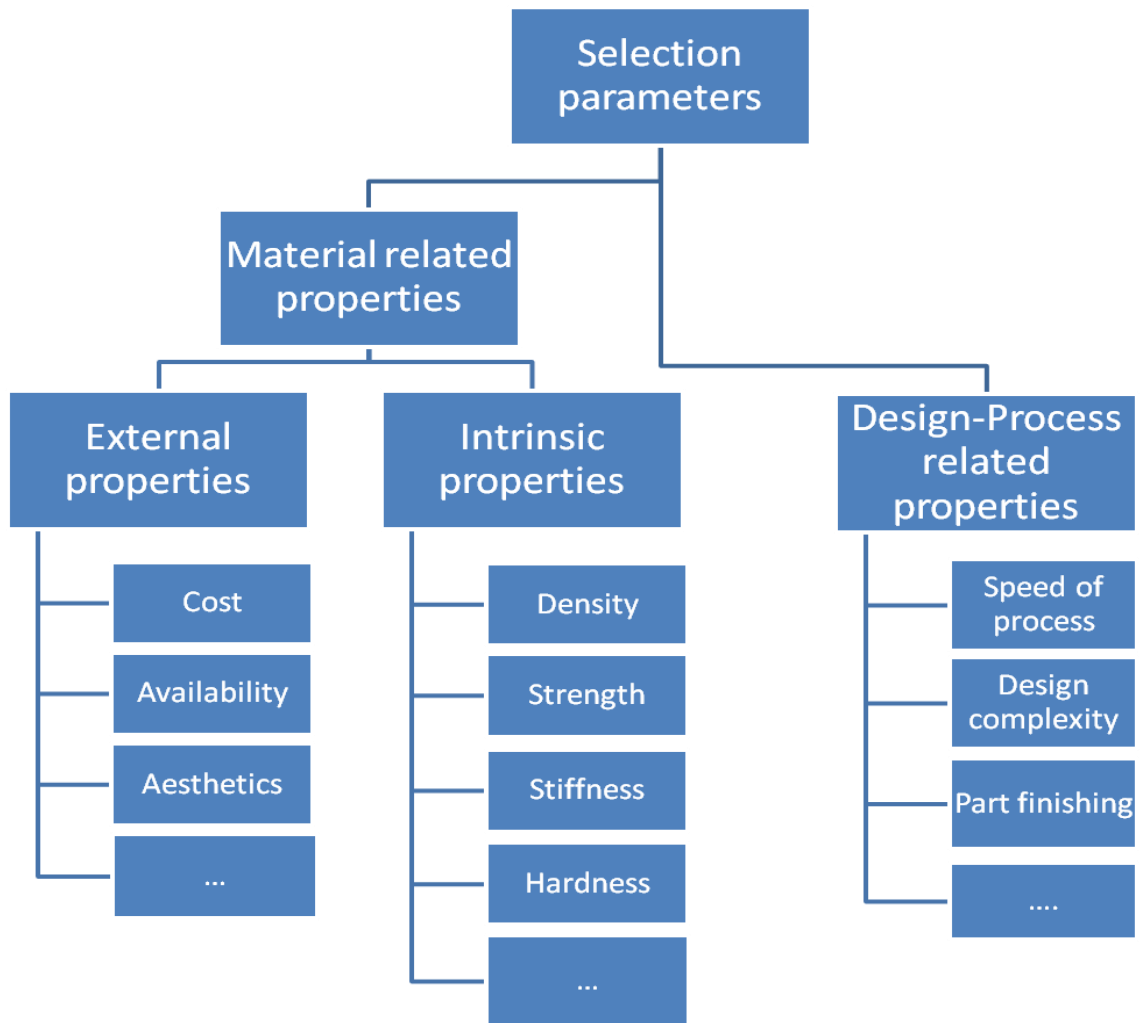


Figure 3.1: Selection parameters

### 3.1 Initial Theoretical Model

From the mechanistic properties briefly discussed above, elastomeric properties were selected to be studied in greater detail as they can be included in a wide range of applications to produce living hinges, snap fits, seals, shock-absorbers etc. While different features ideally require a unique set of material properties, most of the features which make use of the elastomeric properties require the material to bend, stretch or compress. The objective of the initial study was to understand the kinematics of the bending mechanism which could be used in features such as elastic hinges and subsequently find a suitable AM material which would be able to undergo the maximum amount of bending before failure by yield or fracture and be able to withstand a small amount of load. The best material is the one, which for given ligament dimensions, bends to the smallest radius without yielding or failing (Ashby, 2005).

When a ligament of thickness  $2t$  is bent elastically to a radius  $R$ , the surface strain is

$$\varepsilon = \frac{t}{R} \quad (3.1)$$

Assuming that the bending is initially elastic, the maximum stress is

$$\sigma = E \frac{t}{R} \quad (3.2)$$

This must not exceed the yield or failure strength  $\sigma_f$ . Thus the radius to which the feature can be bent without damage is

$$R \geq t \left( \frac{E}{\sigma_f} \right) \quad (3.3)$$

The best material is the one that can be bent to the smallest radius, that is, the one with the greatest value of the index

$$M_1 = \frac{\sigma_f}{E} \quad (3.4)$$

It should also be able to withstand a certain amount of axial load (F). Assuming that w is the width and 2t is the thickness, the tensile stress in the feature should be

$$\sigma_f \geq \frac{F}{2tw} \quad (3.5)$$

Substituting t in (3.3),

$$R \leq \frac{F}{2w} \left( \frac{E}{\sigma_f^2} \right) \quad (3.6)$$

This gives the second index which should be optimized

$$M_2 = \frac{\sigma_f^2}{E} \quad (3.7)$$

The mechanical properties of some of the important AM processes were collected either through published data or from company representatives and compared using the two material indexes discussed previously. The further in the upper right hand corner of the graph a dot is, the higher are the values of the 2 indexes and the better are the elastomeric properties of the material. The AM materials have been compared to polyethylenes (PE) and polypropelene (PP) which are the conventional types of plastics used in features that require elastomeric properties. Figure 3.2 shows a graphical representation of the results (see Appendix A for details).

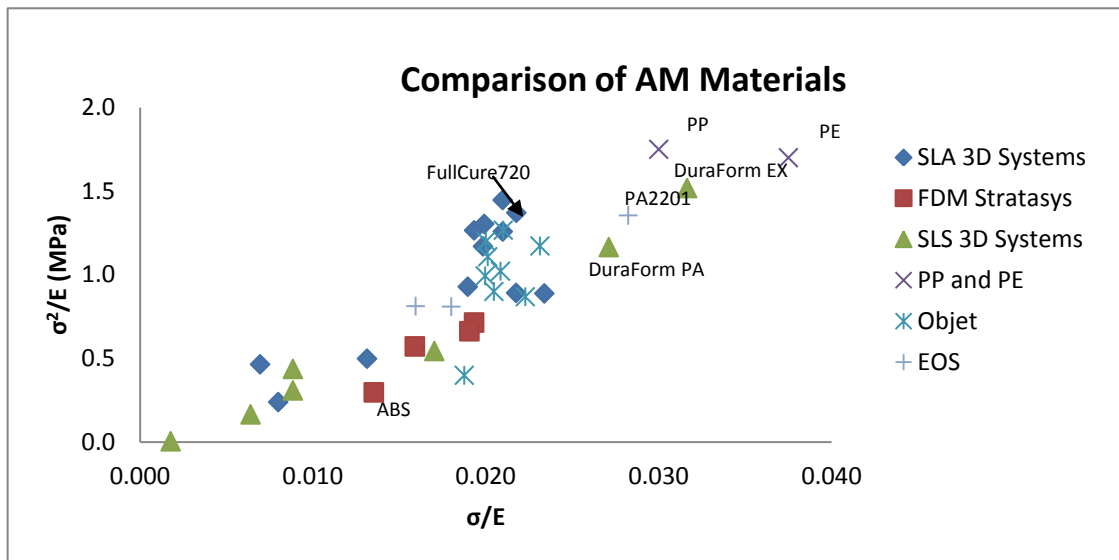


Figure 3.2: Comparison of AM Materials

It is noted from Figure 3.2 that even though PE ( $M_1=0.038$  and  $M_2=1.700$ ) and PP ( $M_1=0.030$  and  $M_2=1.750$ ) have the best elastomeric properties, some of the AM materials like Duraform EX ( $M_1=0.032$  and  $M_2=1.519$ ) from 3D Systems and PA2201 ( $M_1=0.028$  and  $M_2=1.355$ ) from EOS exhibit good elastomeric properties in terms of the 2 indexes chosen. Amongst the Objet materials, FullCure870 ( $M_1=0.023$  and  $M_2=1.173$ ) demonstrates relatively good elastomeric properties. Other Objet materials such as FullCure720 ( $M_1=0.021$  and  $M_2=1.267$ ) show average elastomeric properties. FDM materials from Stratasys and SLA materials from 3D Systems exhibit the worst elastomeric properties as compared to PE and PP. Flex ( $M_1=0.243$  and  $M_2=0.438$ ) and Infiltrated Flex ( $M_1=0.250$  and  $M_2=0.575$ ) from laser sintering 3D Systems which have not been shown in the graph are able to bend very easily but are not able to withstand axial loads. This makes them unsuitable for applications such as living hinges where the structure should be able to withstand small amounts of load.



Based on the analysis, it was determined that FullCure720 from Objet, the AM material available in NUS had sufficient elastomeric properties for living hinges. However preliminary visual tests proved otherwise. The living hinge specimens fabricated using the Objet Eden 350 with FullCure720 failed well before bending 180°. It was noted that only bulk material properties were included in the initial analysis and factors such as feature design and molecular orientation (which also play a role in the final elastomeric properties of the part), have been ignored in this study. For example, some of the critical properties of PP can be improved by enhancing orientation through optimization of the melt temperature and fill speed in injection molding (Elleithy, 2007). Anisotropic effects from AM processes were also ignored in the analysis. It was concluded these approximations might have led to the inaccuracy of the model and that a more refined theoretical model was required along with numerical modeling in order to fully understand the living hinge concept.

### **3.2 Theoretical Living Hinge Model**

The objective of a living hinge is to connect or transmit load between components while allowing relative movement between them by deflecting elastically. It is a thin flexible ligament of material which has its outer fiber under maximum tension and the inner fiber under maximum compression. Traditionally, injection molding has been used to fabricate living hinges. This is because in injection moulding, as the material flows through the narrow gap that is the hinge, the linear molecules align themselves fairly accurately across it, parallel to each other and perpendicular to the axis of the hinge, thereby enhancing orientation and performance. The orientation is further

improved by stretching the semi molten material (before the material is crystallized to a significant degree) by flexing the hinge as the mould is opened (Elleithy, 2007).

The design of a living hinge includes a thin section connecting 2 heavier sections. A recess is located in the upper portion of the thin region, to prevent the formation of a notch which could result in hinge breakage. An arc below the thin section allows for flexing and orientation. Figure 3.3 is a cross-section of a hinge showing its principal dimensions:

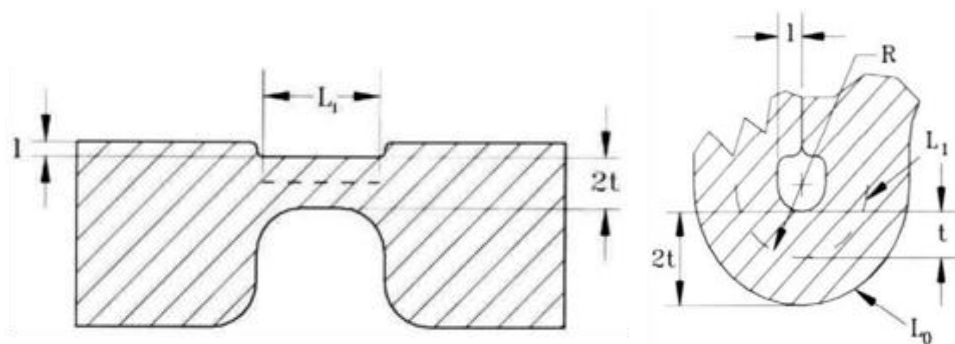


Figure 3.3: Principal dimensions of the living hinge

$L_1$  = length of the neutral axis of the living hinge

$L_0$  = length of the outer lower fiber of the hinge

$R$  = hinge radius

$t$  = half of the hinge thickness

$l$  = recess depth

It is assumed that:

1. The material is anisotropic
2. The tensile yield stress and the compressive yield stress are equal

3. The ultimate tensile stress and the ultimate compressive stress are equal
4. The hinge bends in a circle
5. The total bending angle is  $\pi$

### 3.2.1 Elastic Bending

The length of the neutral axis is the perimeter of the semicircle (Figure 3.3):

$$L_1 = \pi R \quad (3.8)$$

Therefore after the hinge is closed,  $L_0$  the length of the outer lower fiber of the hinge:

$$L_0 = (R + t)\pi \quad (3.9)$$

The strain due to bending is:

$$\varepsilon_{bending} = \frac{\Delta L_0}{L_1} = \frac{t}{R} \quad (3.10)$$

Replacing (3.8) in (3.10),

$$\varepsilon_{bending} = \frac{\pi t}{L_1} \quad (3.11)$$

Assuming that the neutral axis remains at the center, the stress due to bending is:

$$\sigma_{bending} = E \varepsilon_{bending} = E \frac{\pi t}{L_1} \quad (3.12)$$

To have only **elastic** stress and strain,

$$\sigma_{bending} < \sigma_{yield} \quad (3.13)$$

$$E \frac{\pi t}{L_1} < \sigma_{yield} \quad (3.14)$$

Therefore, in order to have only elastic strain, the minimum length  $L_1$  should be:

$$L_1 > E \frac{\pi t}{\sigma_{yield}} \quad (3.15)$$

### 3.2.2 Plastic Bending

Plastic bending will occur when the material is past its elastic phase but has not failed yet. To have plastic bending:

$$\varepsilon_{bending} < \varepsilon_{ultimate} \quad (3.16)$$

Therefore, in order to have plastic strain without failure, the minimum length  $L_1$  should be:

$$L_1 > \frac{\pi t}{\varepsilon_{ultimate}} \quad (3.17)$$

### 3.2.3 Minimum Hinge Thickness

From beam theory, the maximum moment during bending is given by:

$$M < \sigma_{yield} b t^2 \quad (3.18)$$

$$t > \sqrt{\frac{M}{\sigma_{yield} b}} \quad (3.19)$$

### 3.3 Theoretical Modeling of Fullcure720

The published material properties of FullCure720 are:

Property	ASTM	Results in Metric Units	
Tensile Strength	D-638-03	MPa	60.3
Modulus of Elasticity	D-638-04	MPa	2870
Elongation at Break	D-638-05	%	20
Flexural Strength	D-790-03	MPa	75.8
Flexural Modulus	D-790-04	MPa	1718
Compressive Strength	D-695-02	MPa	84.3
Izod Notched Impact	D-256-06	J/m	21.3
Shore Hardness	Scale D	Scale D	83
Rockwell Hardness	Scale M	Scale M	81
HDT at 0.45 MPa	D-648-06	°C	48.4
HDT at 1.82MPa	D-648-07	°C	44.4
Tg	DMA, E''	°C	48.7
Ash Content	NA	%	<0.01
Water Absorption	D570-98 24 Hr	%	1.53

Table 3.1: Material properties of FullCure720

As described earlier, (3.15) provides the inequality for pure elastic bending:

$$L_1 > E \frac{\theta t}{\sigma_{yield}}$$

Taking the bending angle  $\theta = \pi/2$ :

$$L_1 > E \frac{\pi t}{2\sigma_{yield}} \quad (3.20)$$

Replacing the values from Table 3.1 into (3.20):

$$L_1 > 74.765t \quad (3.21)$$

The maximum moment applicable on the living hinge depends on the feature design and usage. Assuming maximum moment to be 1Nmm, the thickness  $2t$  is given by:

$$2t > 0.26 \text{ mm} \quad (3.22)$$

(3.21) and (3.22) are graphically represented in Figure 3.4. The dimensions of living hinge should be in the grey region for it to be able to bend  $90^\circ$  elastically. Going along (i), the length ( $L_1$ ) increases at a constant thickness ( $t$ ) making the hinge more flexible. On the other hand, moving along (iii) increases the thickness ( $t$ ) more than the increase in length ( $L_1$ ) which allows the hinge to support greater loads. Going along (ii) just makes the hinge bigger without necessarily affecting its performance.

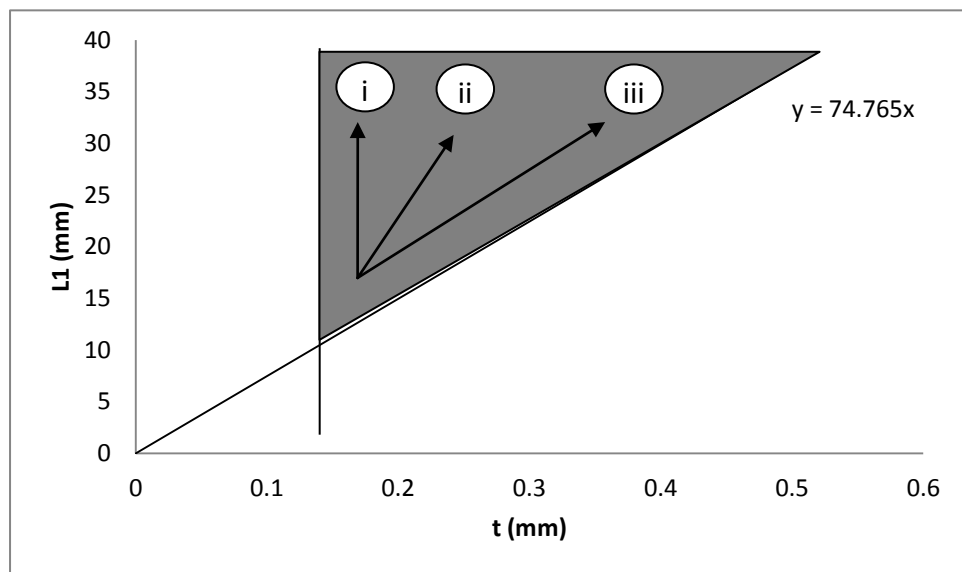


Figure 3.4: Theoretical model of FullCure720

Assuming that  $2t = 0.3 \text{ mm}$  and  $l = .2 \text{ mm}$ ,

$$L_1 > 11.22 \text{ mm} \quad (3.22)$$

It is not impossible to build a practical simple living hinge with  $L_1 = 11.22$  mm and thickness 0.3 as it would be too long. Therefore it is assumed that some amount of plastic bending will take place.

$$L_1 > \frac{\pi t}{2\varepsilon_{ultimate}}$$

$$L_1 > 1.178 \text{ mm} \quad (3.23)$$

The hinge specimens are therefore fabricated with length 1.5 mm, thickness 0.3 mm and recess 0.2 mm.

## Chapter 4. Experimental Study of Material Properties

The Objet Eden 350 (Figure 4.1) machine which uses the PolyJet Matrix 3D Printing technique was chosen for the study due to its availability and potential. The PolyJet Matrix technique has in recent years provided a much cheaper alternative to SLA with similar process specifications. The Eden machines can only print one material at a time but the more recent and more expensive Connex machines provide multi-material capability. The Eden 350 machines provide a tray size of 350x350x200mm (X x Y x Z) with a build resolution of 600 dpi along the X and Y axis and 1600 dpi along the z axis which translates into a layer thickness of 16 $\mu$ . It supports a wide range of materials such as FullCure720, VeroWhite, VeroBlue, VeroBlack and TangoBlack (Objet, 2010). Photopolymers are deposited in layer by the print-head which are then cured by ultra-violet light immediately producing fully cured models without the need for post-curing. The support material, which is also a photopolymer but undercured and this softer, is removed by washing it away with pressurized water in a secondary operation using the apparatus shown in Figure 4.2 (Gibson et al, 2010).



Figure 4.1: Eden 350 (Source: Objet)





Figure 4.2: Water pressure apparatus for removing support structures

FullCure 720 was chosen as the material for the investigation. It is a translucent acrylic-based photopolymer material developed for Objet PolyJet-based 3D Printers. It is relatively rigid compared to DurusWhite FullCure 430 and is conventionally used to build rigid models where internal details are required (Objet, 2010). The material does not require any subsequent machining, has a high elongation at break and good flexural toughness (Pilipovic et al, 2007). Palli et al (2009) used FullCure 720 to successfully build integrated robotic fingers using pin joints that showed very good reliability and more importantly, did not fail after one hundred thousand working cycles.

Studies have shown that photopolymers exhibit changes in mechanical properties with ageing and exposure to sunlight. This may be caused due to the low temperature range exhibited by photo-polymers or by the reaction of the radicals in the occluded sites with diffused oxygen or another reactive species (Gibson et al, 2010). Parts produced in different batches may exhibit different material properties due to difference in the

calibration values of the resin and curing agent. The intensity of the UV light used to cure the photopolymer which depends on the supply voltage can vary the material property of the part. Also, in order to fully understand the elastomeric properties of a material, it is imperative to have the full stress-strain curve of the material which was not publicly available for FullCure 720. Consequently, it was decided that test specimens of the FullCure720 would be prepared along with the feature parts to ensure accurate numerical modeling.

#### 4.1 Specimen Fabrication

All the specimens were fabricated together to avoid differences in mechanical properties due to calibration, intensity of UV light, etc. They were stored together for ten days at room temperature and then tested together to offset the aging effects. There is some inherent anisotropy in the parts fabricated using the PolyJet process which may have been due to the layer-wise nature of the process. The specimens were fabricated in the same orientation to avoid any differences due to orientation. Figure 4.3 represents a screenshot of the software Objet Studio with the specimens.

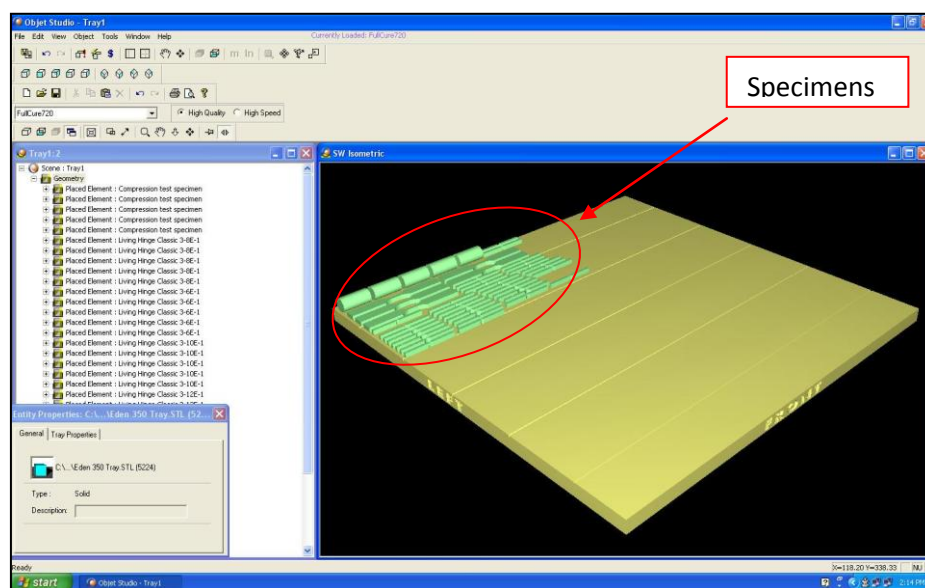
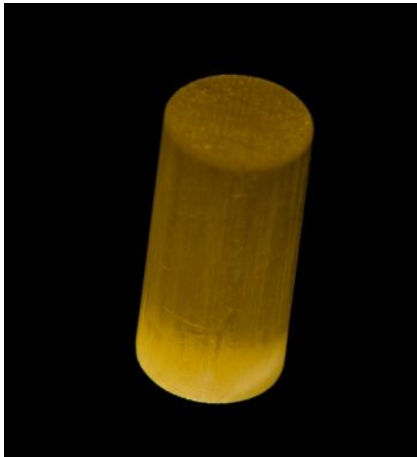


Figure 4.3: Objet Studio

#### 4.1.1 Compression Specimen

5 compression specimens were fabricated in compliance with the ASTM D695-02 Standard Test Method for Compressive Properties of Rigid Plastics. Cylindrical specimens of diameter 12.7 mm (0.5 in) and length 25.4 mm (1 in) were prepared. Special care was taken to ensure that the end faces of these specimens were finished properly so that they were perpendicular to the longitudinal axis of the specimen. Grease was also applied on the top and bottom surface of specimen for reducing friction. The dimensions of the test specimens were measured using the Mitutoyo digital caliper with the measurement range 0-150/0.01 mm. They are presented in Table 4.1.



Compression specimens		
	Diameter	Length
	mm	mm
<b>Theoretical</b>	<b>12.70</b>	<b>25.40</b>
Specimen 1	12.45	25.39
Specimen 2	12.39	25.36
Specimen 3	12.39	25.39
Specimen 4	12.41	25.39
Specimen 5	12.45	25.41
<b>Average</b>	<b>12.42</b>	<b>25.39</b>
<b>Standard Deviation</b>	<b>0.0303</b>	<b>0.0179</b>

Table 4.1: Dimensions for determining compressive properties of specimens

It was noted that the dimensions along the longitudinal axis are more accurate as compared to the dimensions along the other axis. This may be due to calibration errors in the conversion from CAD file to STL file or due to calibration errors in the Objet Eden 350 machine. Since the standard deviation is low and the material properties (stress-strain curves) are calculated based on the actual values which would offset the error, the issue was not investigated further.

### 4.1.2 Uniaxial tension specimen

5 dog-bone shaped uniaxial tension specimens were fabricated in compliance with the D638-03 Standard Test Method for Tensile Properties of Plastics. Table 4.2 presents the principal theoretical dimensions of the specimens.

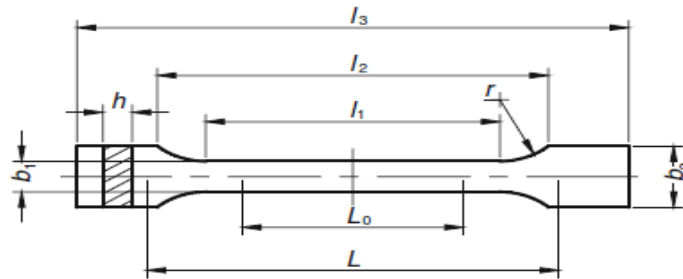


Figure 4.4: Shape of test specimen for tensile testing

	<b>Dimensions</b>
	<b>mm</b>
$l_3$ = total length	85.40
$l_1$ = length of the narrow parallel part	9.53
R = radius	12.70
$l_2$ = distance between expanded parallel part	23.40
$b_2$ = width at the end	9.53
$b_1$ = width of the narrow end	3.18
H = thickness	4.00
$L_0$ = measurement length	8.00
L = initial distance between the machine jaws	45.40

Table 4.2: Principal theoretical dimensions of tensile specimens

As with the compressive test specimens, the dimensions of the tensile test specimens were measured using the Mitutoyo digital caliper with the measurement range 0-150/0.01 mm. They are presented in Table 4.3. Figure 4.5 shows a photograph of the actual specimen.

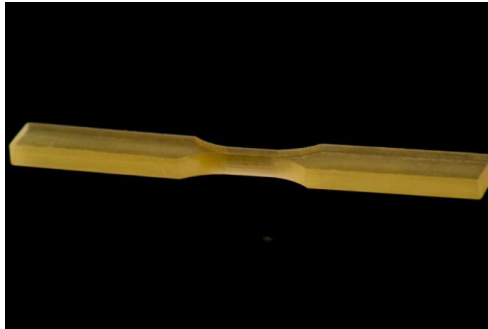


Figure 4.5: Photograph of actual specimen

Tensile Specimens				
	$l_1$	$l_3$	$h$	$b_1$
	mm	mm	mm	mm
<b>Theoretical</b>	<b>9.53</b>	<b>85.40</b>	<b>4.00</b>	<b>3.18</b>
Specimen 1	9.30	85.37	3.70	2.90
Specimen 2	9.30	85.42	3.71	2.91
Specimen 3	9.29	85.40	3.71	2.90
<b>Average</b>	<b>9.30</b>	<b>85.40</b>	<b>3.71</b>	<b>2.90</b>
<b>Standard Deviation</b>	<b>0.0058</b>	<b>0.0252</b>	<b>0.0058</b>	<b>0.0058</b>

Table 4.3: Dimensions for determining compressive properties of specimens

2 specimens presented warpage due to differential shrinkage and could not be used as a result. It was once again noted that the dimensions along the longitudinal axis were more accurate as compared to the dimensions along the other axis.

## 4.2 Testing Procedure

All experiments were carried out on an INSTRON AG-25TB uniaxial mechanical testing machine. The tests were performed at a very low strain rate of  $1.3 \times 10^{-3} \text{ s}^{-1}$ . The controller was set-up in displacement control mode by suitably adjusting the PID parameters. Load and displacement readings along with time were recorded at a sampling rate of 50 samples per second.

### 4.2.1 Compression test

The uniaxial compression tests were performed at a fixed actuator rate in displacement control mode up to an engineering strain of 25%. The compression specimen was placed between the push rods as shown in Figure 4.6. Grease was applied on the top and bottom surface of the specimen to reduce friction between the specimen and the loading platens. A 25kN load cell was used to acquire the load data. The load and displacement data were continuously acquired at a sampling rate of 50 samples per second. These were used to compute the engineering stress and strain from which the true stress and true strain was then calculated for each test.

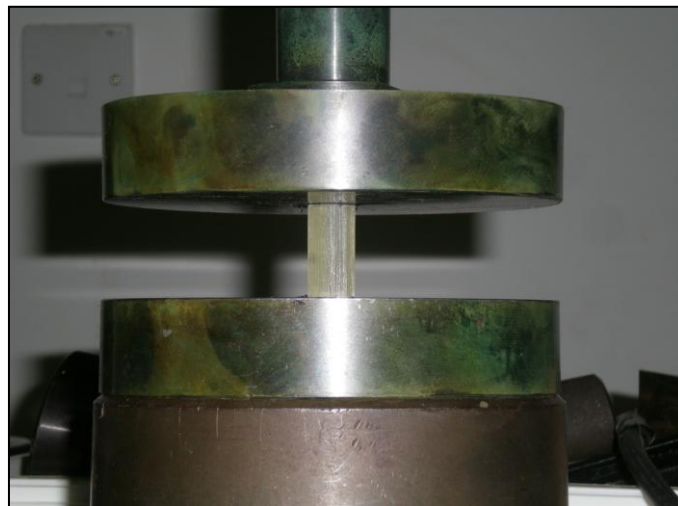


Figure 4.6: Compression test

### 4.2.2 Tensile test

The specimen was fixed on to the INSTRON machine and pulled at a rate of 2mm/min in displacement-controlled mode as shown in Figure 4.7. A 5kN load cell was used to acquire the load data. The load and displacement data were continuously acquired at a sampling rate of 50 samples per second. A strain gauge was also mounted on the central portion of the specimen to measure the displacement for the

last test. This was recorded through one of the channels of the data acquisition system. These were used to compute the engineering stress and strain from which the true stress and true strain was then calculated for each test.



Figure 4.7: Tensile test

## 4.3 Results and Discussion

### 4.3.1 Compression tests

Two specimens were used as trial specimens to understand the functioning of the machine and to calibrate it. The load-displacement data obtained from them was not considered. The engineering stress-strain curves determined from the other three specimens are plotted in Figure 4.8. The tests were conducted at room temperature with a displacement rate of 2 mm/min. The results presented clearly show repeatability of the data.

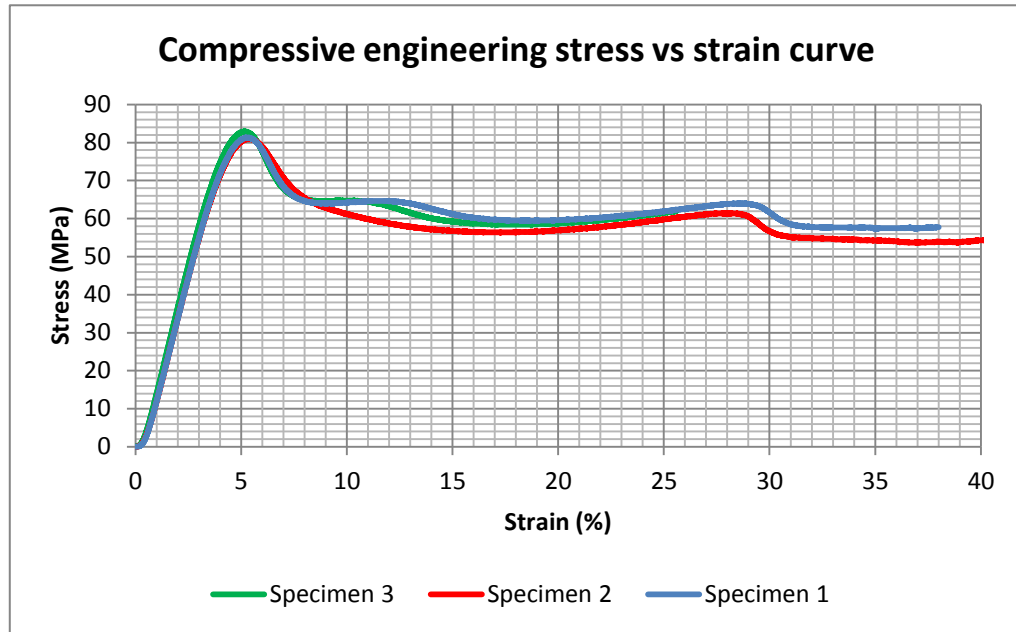


Figure 4.8: Compressive engineering stress vs strain curve

It was noted that the stress-strain curve in Figure 4.8 exhibits a reversal of curvature indicating a softening phase over small strains followed by a hardening phase for larger strains. To compensate for the toe region, stresses  $\sigma_1$  and  $\sigma_2$  corresponding to the strain values  $\varepsilon_1 = .01$  and  $\varepsilon_2 = .05$  were recorded (Pilipovic et al, 2007) and the Young's modulus was calculated using the relation:

$$E = \frac{\sigma_2 - \sigma_1}{\varepsilon_2 - \varepsilon_1} \quad (4.1)$$

The Young's modulus was calculated to be 1715.8 MPa with a standard deviation of 5.47. A straight line passing through the 1% strain was drawn parallel to the slope of the initial linear part of the curve. The point of intersection of this straight line passing through the 1% strain and the stress versus strain curve was considered to be the yield point and the stress corresponding to this yield point is treated as the yield stress. The yield strength value was obtained as 81.7 MPa with a standard deviation of 0.84. The experimental results obtained after 25% strain are not included in the calculations due



to the barreling of the specimen considering this as failure. The true stress versus logarithmic strain curve was obtained from the engineering stress versus strain curve using the relations:

$$\varepsilon_t = \ln(1 + \varepsilon_e) \quad (4.2)$$

$$\sigma_t = \sigma_e(1 + \varepsilon_e) \quad (4.3)$$

The subscripts t and e refer to true and engineering respectively. Figure 4.9 shows a plot of the true stress versus logarithmic strain curve.

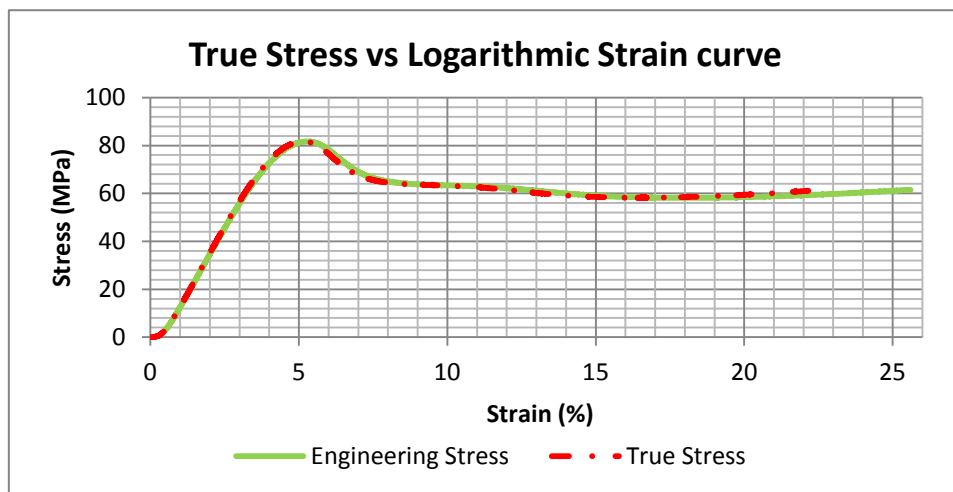


Figure 4.9: True stress vs logarithmic strain

### 4.3.2 Tensile tests

The engineering stress versus strain curve obtained from the load-displacement data plot is shown in Figure 4.10. The tests were conducted at room temperature with a displacement rate of 2 mm/min. The results presented clearly show repeatability of the data.

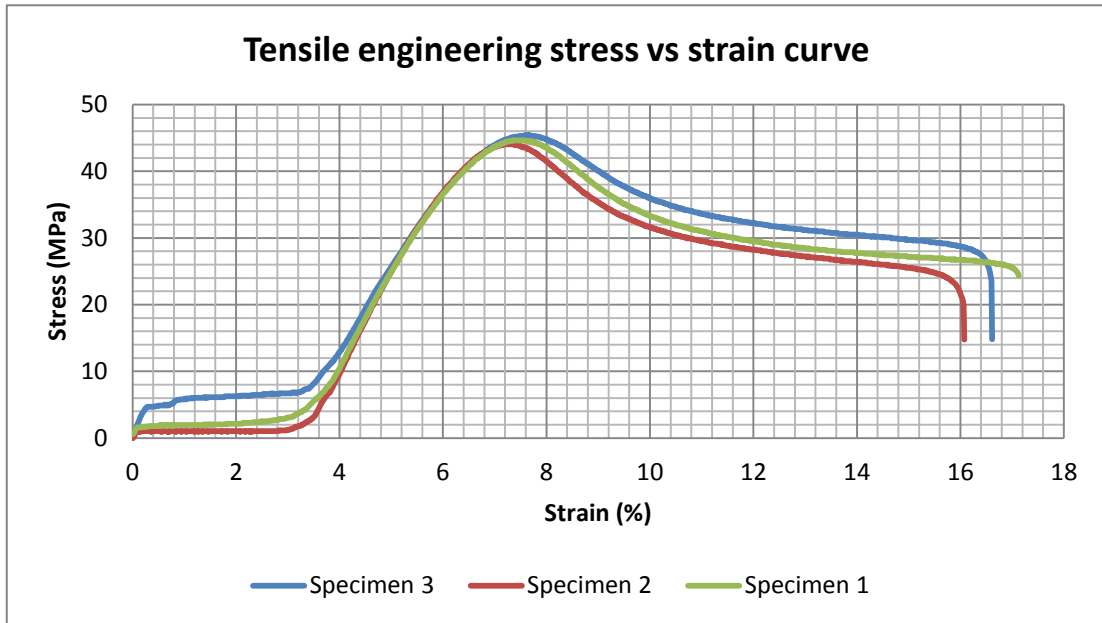


Figure 4.10: Tensile engineering stress vs strain curve

It was noted from Figure 4.10 that the stress versus strain curve exhibits an unusually long toe region of 3.3% strain and an absolute displacement of 0.8 mm. This could be due to slippage since the displacement data from the INSTRON machine was used to calculate the strain instead of a strain gauge. Another test was conducted with a strain gauge, the results of which did not exhibit any toe region suggesting that the original results might have been distorted due to slippage. However the complete stress-strain curve could not be obtained using the strain gauge since the model available for the required dimensions in NUS could only record strain up to 2%. It was decided that the true stress versus logarithmic strain curves for FullCure720 under compression will be used in Chapter 5 to build the numerical model.

## Chapter 5. Numerical Analysis

The objective of this part of the study was to develop a general Finite Element Analysis (FEA) model taking living hinges as an example which could be used to model different features that make use of the elastomeric properties of FullCure 720 or similar materials. The study investigated the high deformation which occurs during the bending of a feature and examined the ability of FEA to predict the feature behavior by obtaining simulation results from a model that undergoes high element distortion. The analysis included the modeling of the geometry and boundary conditions replicating the experiment described earlier, the material properties obtained from the compression tests and structured mesh elements to calculate the contact forces which were compared to the results obtained from the experiments.

Unlike in most metals (Hill, 1967), deformation in polymers is very sensitive to hydrostatic pressure. The effect of pressure can be seen in the difference observed between stress-strain curves in both uniaxial tension and compression which are associated with a negative and positive pressure respectively (Rabinovitz et al, 1974). This effect also leads to a pressure dependence of the yield stress (Bardia and Narasimhan, 2006). Based on the response of many polymers under different states of stress (tension, compression, plane strain compression, etc.), it has been deduced that their plastic yielding is affected by the local normal stress and/or the hydrostatic stress (Bauwens, 1970). This behavior can be explained by assuming a

pressure-dependent yield criterion. Consequently, three such criteria have been suggested to describe yielding in polymeric solids (Bowden and Jukes, 1972):

- Drucker-Prager
- Mohr Coulomb
- Modified Tresca

Polymers which exhibit heterogeneous deformation due to occurrence of shear bands during plastic deformation (such as polystyrene (PS), polyethylene (PET), etc), are closely approximated by Mohr-Coulomb or modified Tresca criteria. Polymers such as polymethacrylate (PMMA), polyvinyl chloride (PVC), epoxy resins, etc undergo a more homogeneous plastic deformation and can be approximated by Drucker-Prager criterion. Polymers that do not exhibit sensitivity to hydrostatic pressure can be closely approximated using von Mises yield criterion (Du Bois et al, 2005).

Documentation on FullCure 720 provided by Objet Inc specifies that the compressive yield stress of FullCure 720 is 1.4 times higher than the tensile yield stress. This indicated pressure-sensitive yielding which made it impossible to fall under the von Mises criterion. Even though the PolyJet process exhibits a small amount of anisotropy due to the layer-wise fabrication process, the anisotropy is small as compared to other processes and not well documented. Thus, FullCure 720 was isotropic and the original linear Drucker Prager (DP) model was used to describe the constitutive response of a material that exhibits pressure sensitive yielding in conjunction to the linear elastic model.

The DP yield function is attractive from the standpoint of numerical implementation since it has a continuously varying normal. The DP model may be extended to include the effect of  $J_3$  in addition to  $J_2$  and hydrostatic stress. In this extended form, it can be used to represent the constitutive response of a wide variety of materials such as soils, rocks, ceramics, polymers and metallic glasses. A general feature of these materials is that the compressive and tensile yield strengths are significantly different. Three different yield criteria can be obtained from this model. These differences are based on the shape of the yield locus in the meridional plane which may be a linear, hyperbolic or a general exponent form. In this work, the linear DP model is used.

The extended DP yield function is given as:

$$\phi(\sigma_{ij}, \sigma_c) = \frac{q}{2} \left[ 1 + \frac{1}{c} - \left( 1 - \frac{1}{c} \right) \left( \frac{r}{q} \right)^3 \right] + \sigma_m \tan \beta - \left( 1 - \frac{1}{3} \beta \right) \sigma_c = 0 \quad (5.1)$$

where,

$$\sigma_m = \frac{1}{3} (\sigma_1 + \sigma_2 + \sigma_3) \quad (5.2)$$

$$q = \sqrt{3J_2} \quad (5.3)$$

$$r^3 = \frac{27}{2} J_3 \quad (5.4)$$

Here  $(\sigma_1 + \sigma_2 + \sigma_3)$  are the principal values of the Cauchy stress tensor  $\sigma_{ij}$ ,  $J_2$  and  $J_3$  are the second and third invariants of the deviatoric part of the Cauchy stress, and  $\sigma_m$  is hydrostatic stress. Furthermore,  $\sigma_c$  is the true yield stress in a

uniaxial compression test and  $\beta$  and  $C$  are material parameters. Figure 5.1 shows a schematic representation of the yield function. It can be seen that the equation represents a conical surface in principal stress with the vertex on the hydrostatic tension axis.

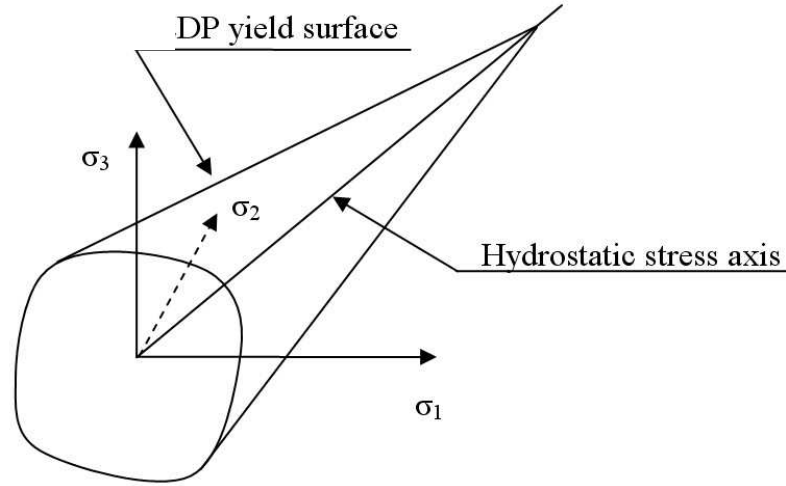


Figure 5.1: Drucker Prager yield function

The shape of the yield surface is determined by the value of  $C$  which is the ratio of the flow stress in tri-axial tension to the flow stress in tri-axial compression. Assuming  $C$  to be 1 gives a circular trace which corresponds to the original DP model. Replacing  $C=1$  in the extended DP equation gives us the following original DP equation which is used in this study:

$$\phi(\sigma_{ij}, \sigma_c) = q + \sigma_m \tan \beta - (1 - \frac{1}{3} \tan \beta) \sigma_c = 0 \quad (5.5)$$

where,

$$\sigma_m = \frac{1}{3}(\sigma_1 + \sigma_2 + \sigma_3) \quad (5.6)$$

$$q = \sqrt{3J_2} \quad (5.7)$$

$\beta$  , the angle of friction is given by:

$$\tan \beta = \frac{3(\alpha - \frac{1}{c})}{\alpha + 1} \quad (5.8)$$

where  $\alpha = \sigma^c / \sigma^t$  is the ratio (true) yield stress in uniaxial compression to that in uniaxial tension.

The total deformation  $D_{ij}$  (symmetric part of the spatial gradient of velocity) is taken to be the sum of an elastic and a plastic part, so that,

$$D_{ij} = D_{ij}^e + D_{ij}^p \quad (5.9)$$

The Jaumann rate of Cauchy stress  $\sigma_{ij}^*$  is related to  $D_{ij}^e$  by a constant, positive definite, isotropic elasticity tensor  $C_{ijkl}$  as

$$\sigma_{ij}^* = C_{ijkl} D_{ij}^e \quad (5.10)$$

The plastic part of the deformation rate  $D_{ij}^p$  is taken to be directed along the normal of a flow potential surface  $G$ , so that

$$D_{ij}^p = \delta \frac{\delta G}{\delta \sigma_{ij}} \quad (5.11)$$

where  $\delta \geq$  is the plastic parameter. The potential surface  $G$  is assumed as:

$$G(\sigma_{ij}) = \frac{q}{2} \left[ 1 + \frac{1}{c} - \left(1 - \frac{1}{c}\right) \left(\frac{r}{q}\right)^3 \right] + \sigma_m \tan \varphi \quad (5.12)$$

Replacing  $C=1$  to get the equation corresponding to the original DP model:

$$G(\sigma_{ij}) = q + \sigma_m \tan \varphi \quad (5.13)$$

In the case of  $\varphi = \beta$ , the normals to yield surface and the flow potential surface will coincide resulting in associated plastic flow which is used in this work.

Solidworks, a parasolid-based solid modeler developed by Dassault Systemes SA was initially used to build the models and carry out the FEA. The following is a screen-shot of the living hinge feature built on Solidworks:

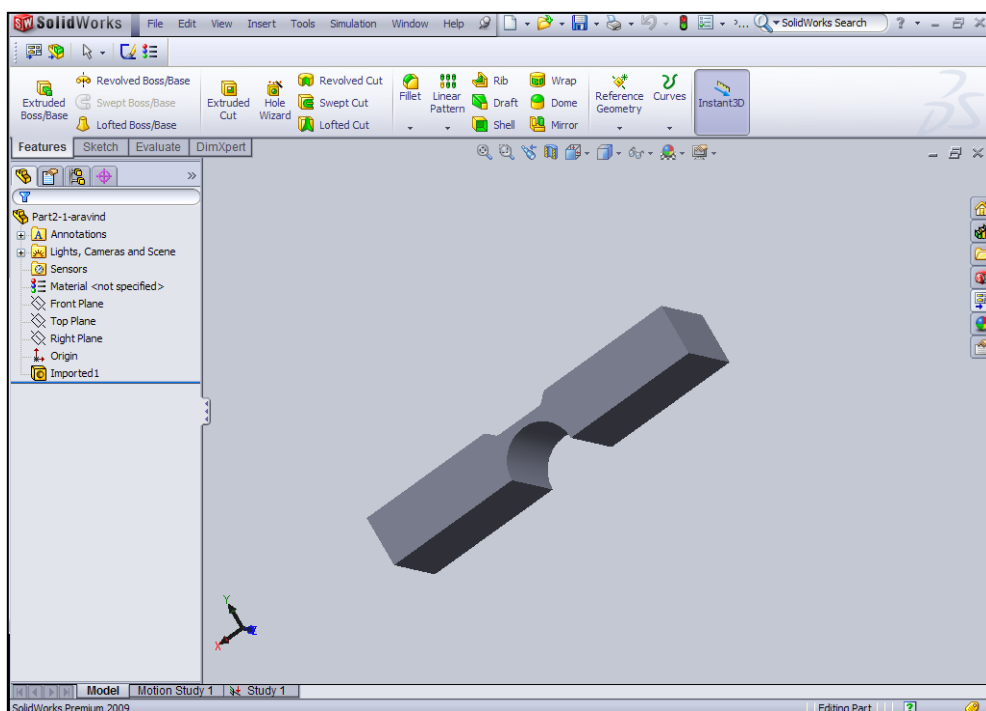


Figure 5.2: Modeling on Solidworks

Solidworks has a component called COSMOS for FEA. The basic version of COSMOS which is available to students in NUS is not suitable for large deformations analysis since it does not allow hydrostatic pressure to be considered. It can be handled to some extent using COSMOS Pro which was not accessible due to financial constraints.



Abaqus/Standard was chosen for the study after examining the large deformation capabilities of various FEA software packages. The Drucker-Prager (DP) model is an in-built constitutive model implemented in the general purpose finite element code ABAQUS. It employs the fully implicit Backward Euler technique for integrating the constitutive equations. For this purpose, material tangent moduli are derived by consistent linearization of the stress update algorithm. The use of consistent tangent moduli in conjunction with the global equilibrium Newton-Raphson (N-R) method results in a quadratic rate of convergence. The global N-R iterations are continued until the convergence criteria in terms of force norm and displacement norm are met to a sufficiently small tolerance.

## **5.1 Initial models**

### **5.1.1 Elastic model**

A simple model of living hinge was developed initially using the default von Mises yield criterion. One end of the living hinge was completely restrained and the bottom face of the other end was subjected to a uniformly distributed pressure. The uniform pressure was modeled as a follower force (normal to the current position of the plane). This ensured that the living hinge would be able to bend 180°. ABAQUS offers the option of both follower force and non-follower force (normal to the initial plane). Figure 5.3 shows a screenshot of the simple living model with the boundary conditions. The material is defined by the Young's modulus (1715 MPa) and the Poisson's ratio was taken to be 0.3 as published by Vesenjok et al.

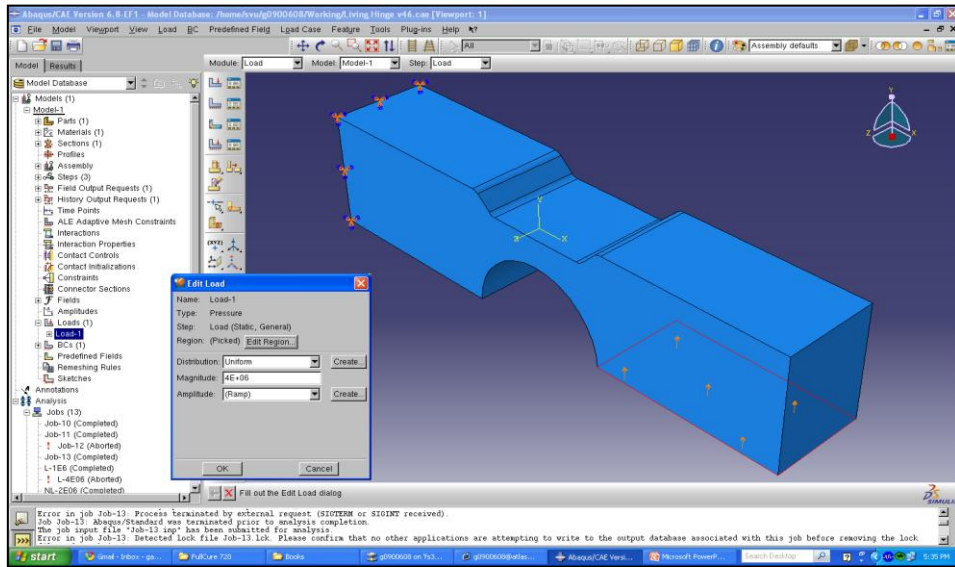


Figure 5.3: Screenshot of the elastic model

A fine mesh was used to avoid shear locking. C3D8R, a general purpose linear brick element with reduced integration was initially used. Reduced integration is a simple way to avoid volumetric locking. In reduced integration, the element stiffness is integrated using an integration scheme that is one order less accurate than the standard scheme. The shape of C3D8R is shown in Figure 5.4 along with the integration point.

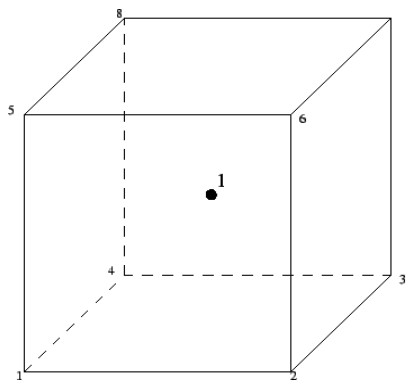


Figure 5.4: Element type C3D8R

However reduced integration led to ‘hourglassing’, as shown in Figure 5.5. Hourglassing is caused by a system of equations which have a weakly constrained deformation mode. There are a number of ways in which hourglass formation can be prevented. Selectively reduced integration works by modifying the formulation for static linear elasticity by treating the volumetric and deviatoric parts of the stiffness matrix separately. The B-bar method additionally modifies the definition of the strain in the element. Hourglassing can also be cured by adding an artificial stiffness to the element that acts to constrain the hourglass mode. Abaqus allows the user to choose element type as hybrid which can also be used to prevent hourglassing. Hybrid elements include the hydrostatic stress distribution as additional unknown variable. The unknown variable must be computed at the same time as the displacement field. This allows the stiff terms to be removed from the system of finite element equations. For this study, hybrid elements (C3D8H) were used which not only cured hourglassing but also prevented the stiffness matrix from getting ill-conditioned.

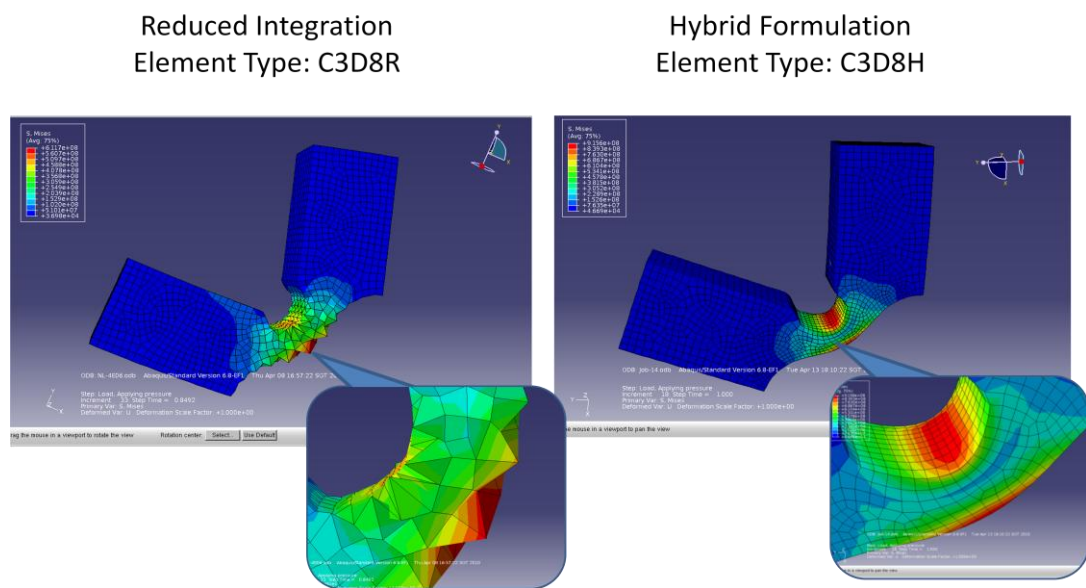


Figure 5.5: Hourglass formation

### 5.1.2 Plastic-Elastic model

The von Mises stress reached 1000 MPa in the elastic model while the yield stress for FullCure 720 was noted to be 80 MPa earlier. Since the stresses were much higher than the yield stress, it meant that an elastic-plastic model would be needed instead of a simple elasticity model. Even though the PolyJet process exhibits a small amount of anisotropy due to the layer-wise fabrication process, the anisotropy is small as compared to other processes and not well documented. Thus FullCure 720 was assumed to be strain-rate independent and undergoing homogenous deformation and the original linear Drucker Prager model with a symmetric stiffness matrix was used with  $\sigma^c/\sigma^t$  as 1.4 in conjunction with the linear elastic model.

The model was unable to provide converging results for the softening phase in the stress-strain curve as seen in Chapter 4. Since the objective of the study was to model the feature behaviour at large deformations and the softening takes place over a relatively small region, the piecewise power law hardening law was used to approximate the stress-strain curve. Using Eqns:

$$\frac{\varepsilon^p}{\varepsilon_y} = \begin{cases} 0 & \sigma \leq \sigma_y \\ \left(\frac{\sigma}{\sigma_y}\right)^n & \sigma > \sigma_y \end{cases} \quad (5.14)$$

where  $\varepsilon^p = \varepsilon - \frac{\sigma_y}{E}$ ,  $\varepsilon_y$  is the yield strain,  $\sigma_y$  is the yield stress and n is a constant which is assumed to be 50. Fig 5.6 shows the resulting approximation.

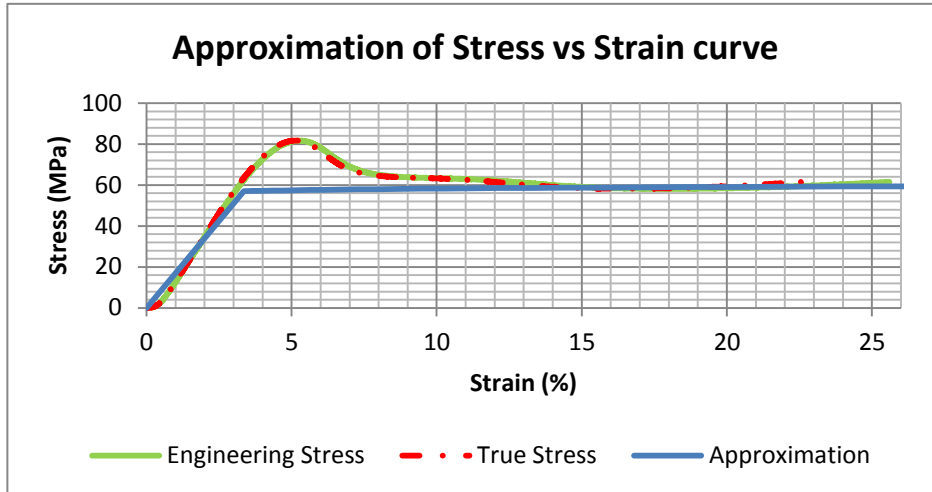


Figure 5.6: Approximation of the stress vs strain curve

The angle of friction or the slope of the linear yield surface in the  $p$ - $t$  stress plane is given by:

$$\tan \beta = \frac{3(\alpha - \frac{1}{C})}{\alpha + 1} \quad (5.15)$$

where  $\alpha = \sigma^c / \sigma^t = 1.4$  and  $C=1$  as explained earlier in the section. Thus  $\beta$  was calculated to be  $26.5^\circ$ .

#### 5.1.2.1 Force Boundary Condition

A uniform pressure was applied on one face of the living hinge. The pressure was a follower force in order to replicate a real life hinge. This was called the Force Control boundary condition since only the amount of force applied was pre-decided and the hinge was allowed to move freely on application of the force. The pressure was increased slowly from 0 MPa to 12 MPa as shown in Fig 5.7:

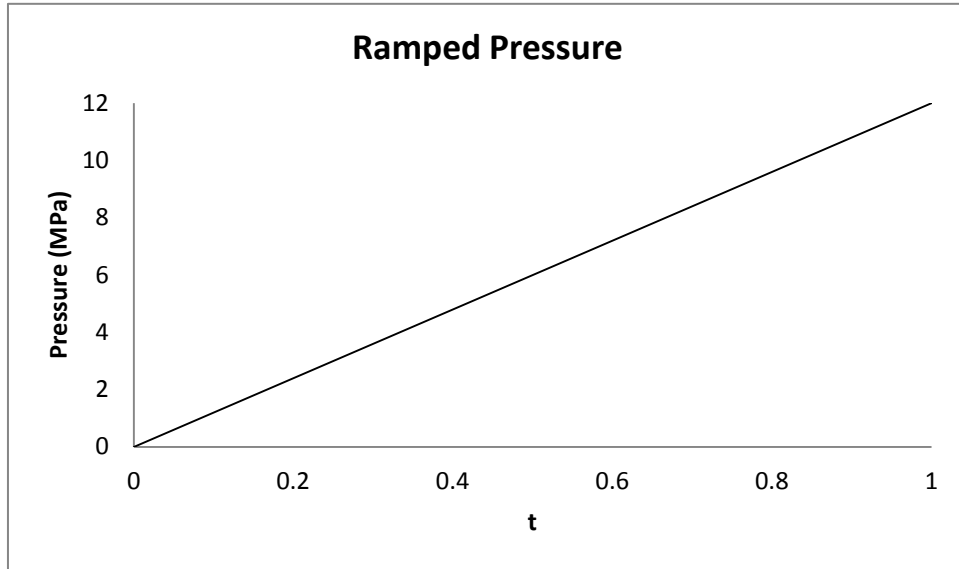


Figure 5.7: Ramped pressure on the living hinge

The Drucker-Prager model with the Force Control boundary condition failed at approximately 85 degrees of rotation. The failure of the solver was possibly because the applied moment was too high for the specimen to sustain. It is very difficult to replicate the exact moment curve required to close the living hinge. It was concluded that in order to solve the problem, we would use a displacement boundary condition instead of a force.

#### 5.1.2.2 Displacement Control Boundary Condition

Instead of defining the force applied on the living hinge, the displacement of the living hinge at different times was provided to ABAQUS in order for it to calculate the reaction forces. This was called the Displacement Control Boundary

condition. However before this approach could be used, there were several issues with this approach which had to be resolved.

Firstly, the point at which the displacement was applied as boundary condition yielded catastrophically due to extremely high reaction force. To resolve the issue the neck region of the living hinge was modeled to be plastic-elastic in to be able to study the reaction force while the rest of the hinge was modeled to be completely elastic. Fig 5.8 illustrates the model set-up.

Also, there are no rotational degrees of freedom allowed in continuum elements. As a result, the displacement had to be defined on a point on the x-y coordinate system. The mid-point of the opposite face of the living hinge as shown in Fig 5.8 was chosen since it was simplest to model.

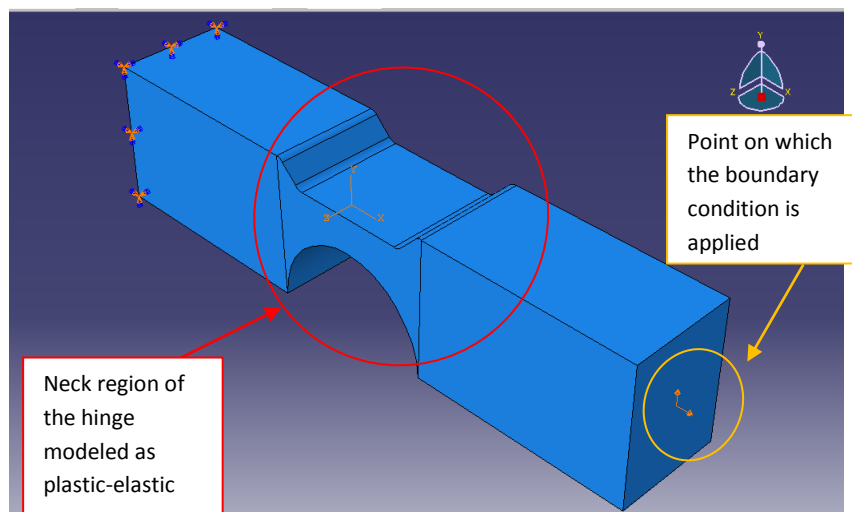


Figure 5.8: Displacement Control Boundary Condition

The displacement of the node was defined by the following equations so that the point traces a semi-circular path (shown in Fig 5.9):

$$u = -R(1 - \cos\theta)$$

$$v = R\sin\theta$$

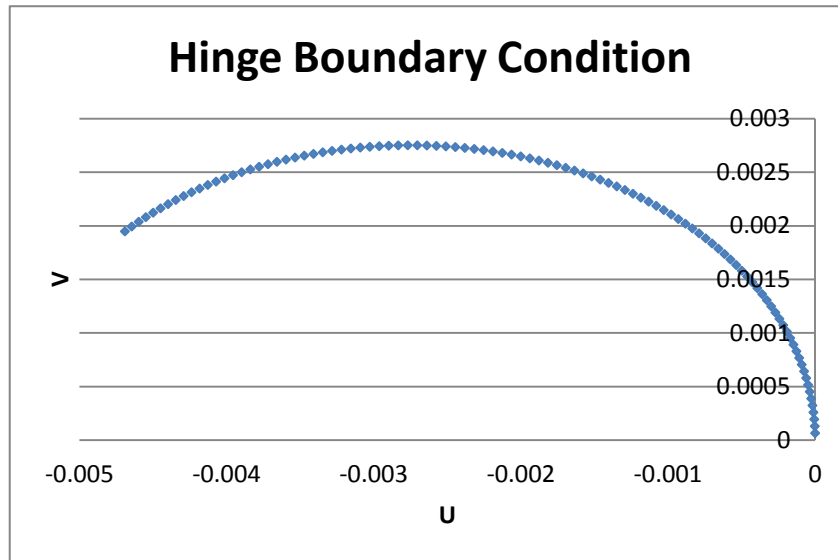


Figure 5.9: Semi-circular path traced by node

The above boundary condition does not take into account the fact there is strain during the bending which changes the radius of curvature of the living hinge. To address the issue, the path followed by the same mid-point node while in the elastic model was taken and used as the boundary condition for the Drucker-Pagar model. Fig 5.10 shows the difference between the path traced by the mid-point node in the elastic model and the path defined by semi-circular equations.



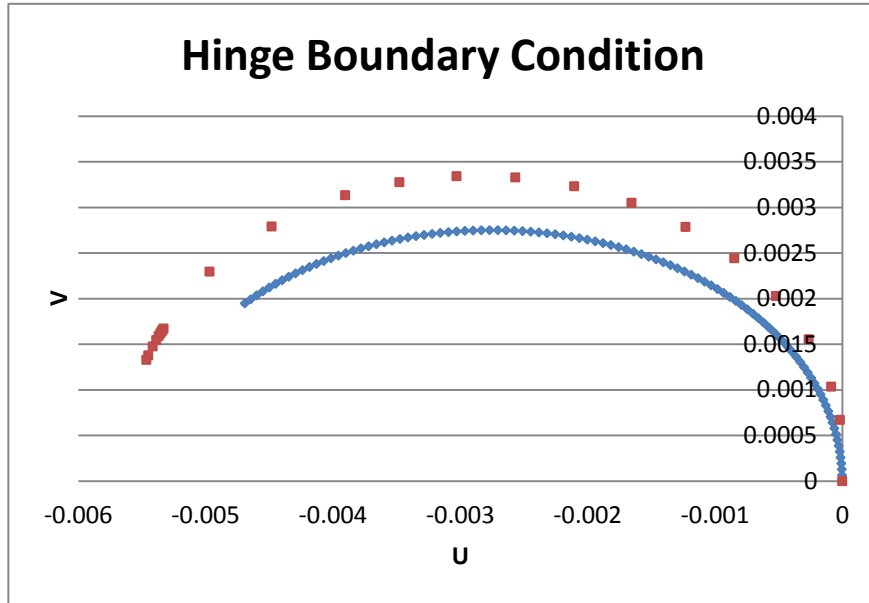


Figure 5.10: Path by mid-point of elastic model vs path by semi-circular equations

A functioning Finite-Element Analysis model as shown in Fig 5.11 was obtained which would be later refined to closely approximate the boundary conditions in the experimental set-up.

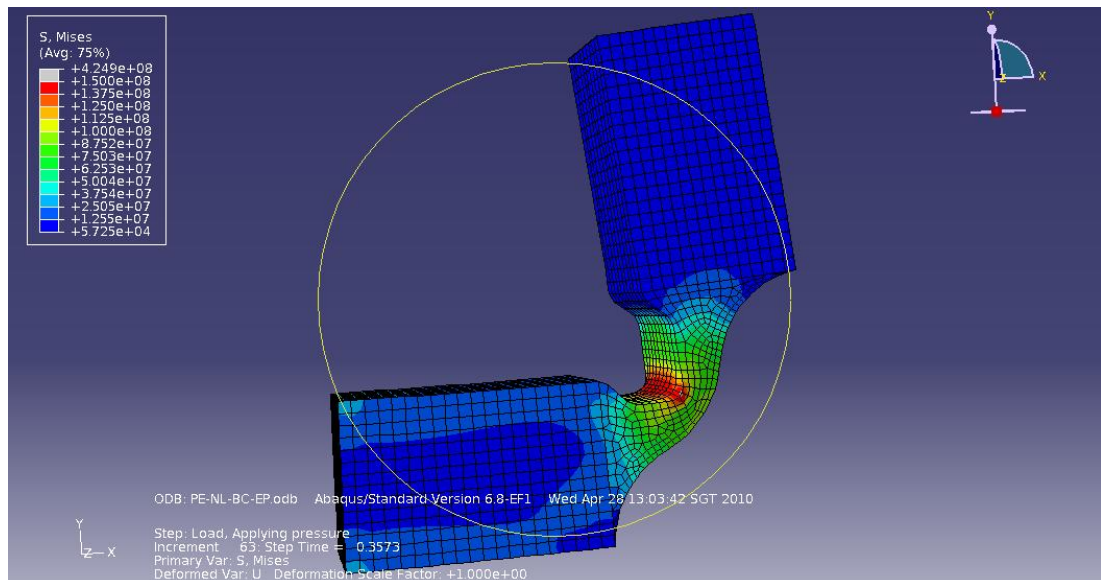


Figure 5.11: Functioning living hinge model

## Chapter 6. Experimental Set-Up

The objective of this part of the study was to develop an experimental set-up that would closely resemble the real life functioning of a living hinge while allowing repeatability and measurability.

Hinge specimens of varying thicknesses of the neck region were fabricated to study their effects on the bending. Figure 6.1 shows the drawing and photograph of a fabricated living hinge specimen.

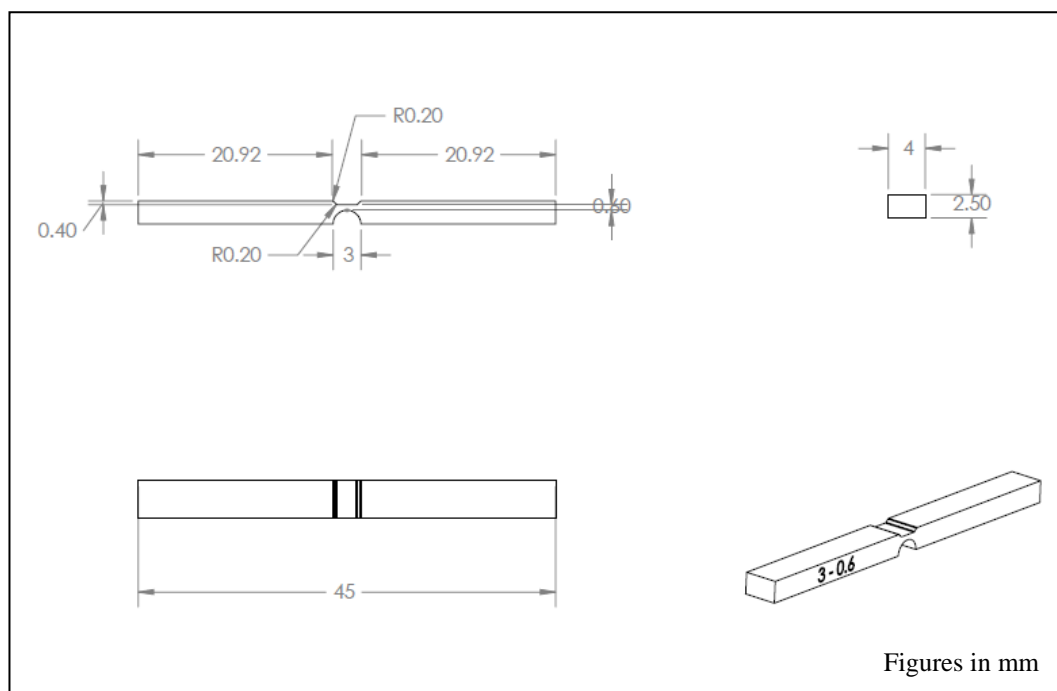


Figure 6.1: Living hinge specimen

The dimensions of the test specimens were measured using the Mitutoyo digital caliper with the measurement range 0-150/0.01 mm. The average thicknesses ( $2t$ ) of the specimen were 0.37 mm, 0.52 mm and 0.70 mm with standard deviation of 0.047, 0.039 and 0.028 respectively. The hinge length ( $L_1$ ) was maintained constant at 3 mm with standard deviation of 0.016. The top recess ( $l$ ) was also maintained constant at 0.40 mm. The height of the specimens was 2.30 mm while the breadth was 3.70 mm. The details of the dimensions of the hinge specimens fabricated are provided in Appendix B.

An L-jig was developed which could be used along with a torsion testing machine to bend a living hinge in a radial path. Fig 6.2 shows the drawing of the jig and Fig 6.3 shows the drawing of the clamp to hold the living hinge specimen.

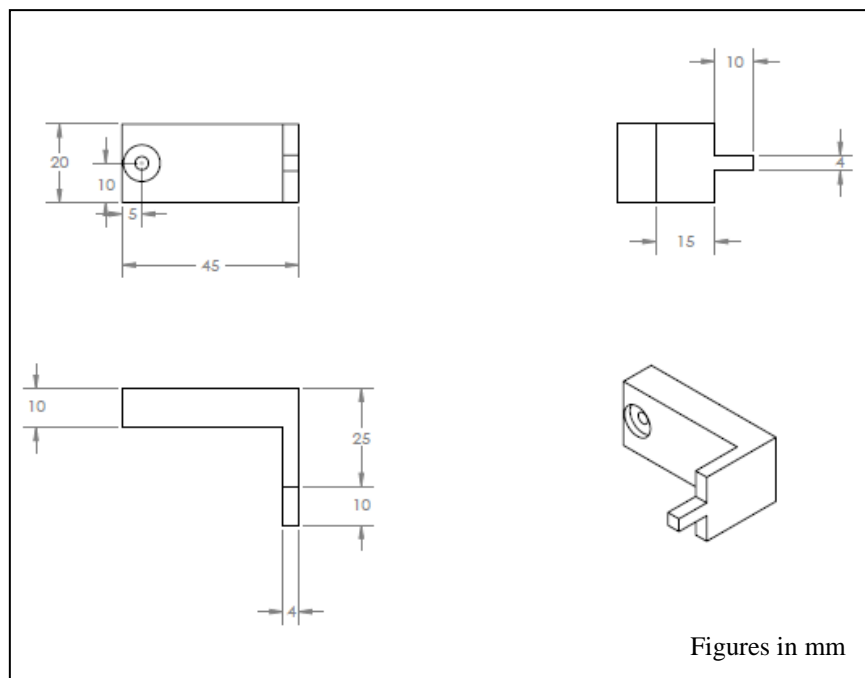


Figure 6.2: L-jig to bend the living hinge specimen in a radial path

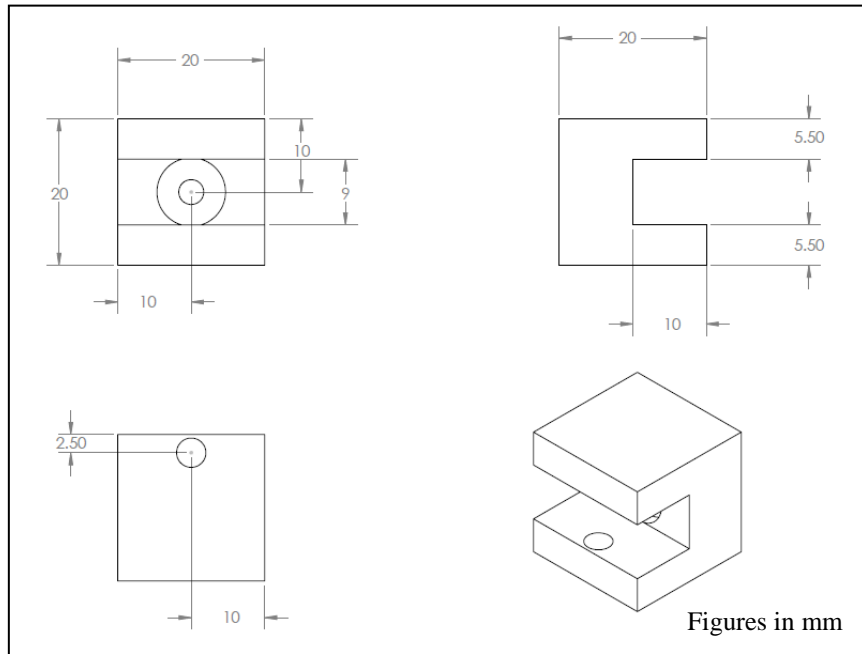


Figure 6.3: Clamp to hold specimen from one end during bending

Preliminary Finite Element Analysis showed that the moment would be in the range of 10-30 Nmm. Even though the torsion test machine in the Applied Mechanics lab was theoretically capable of measuring the moment in the range of 10-30 Nmm, in practice the machine was not sensitive enough. Further investigation showed that such a sensitive torsion machine was not available in Singapore. Scaling up the specimen was also not a viable option since the FullCure 720 is an expensive material.

In order to address the issue, a jig was developed which could be used along with a tensile micro-testing machine to bend the living hinges and record the force vs vertical displacement. Fig 6.4 shows the drawing of the jig and Fig 6.5 and Fig 6.6 show photographs of the set-up.

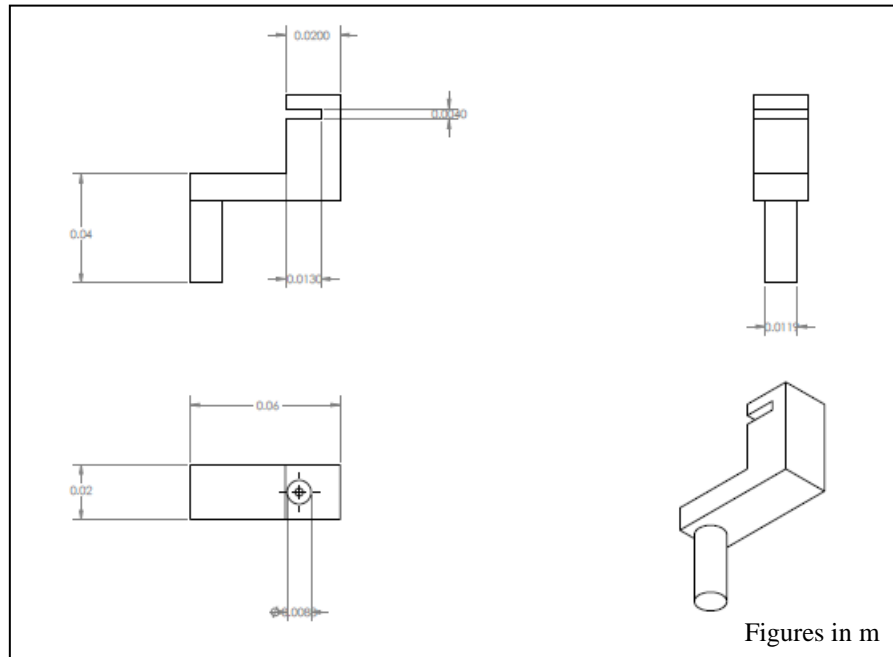


Figure 6.4: Drawing of the jig to bend the hinge in a vertical path

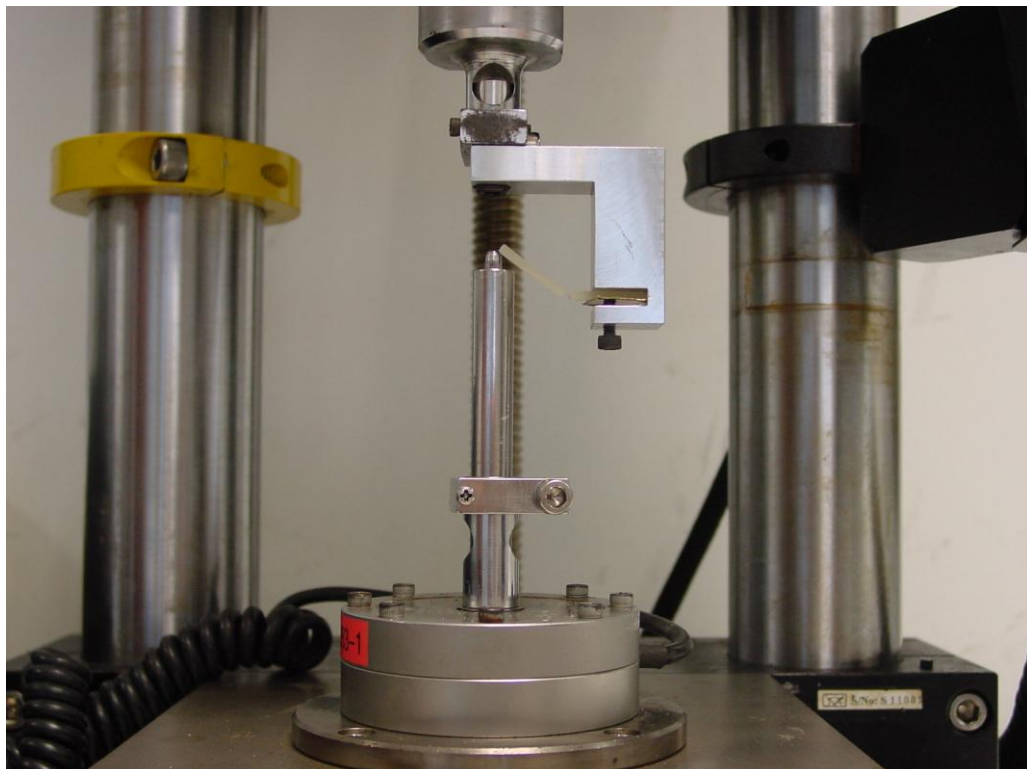


Figure 6.5: Experimental set-up with a tensile micro-testing machine

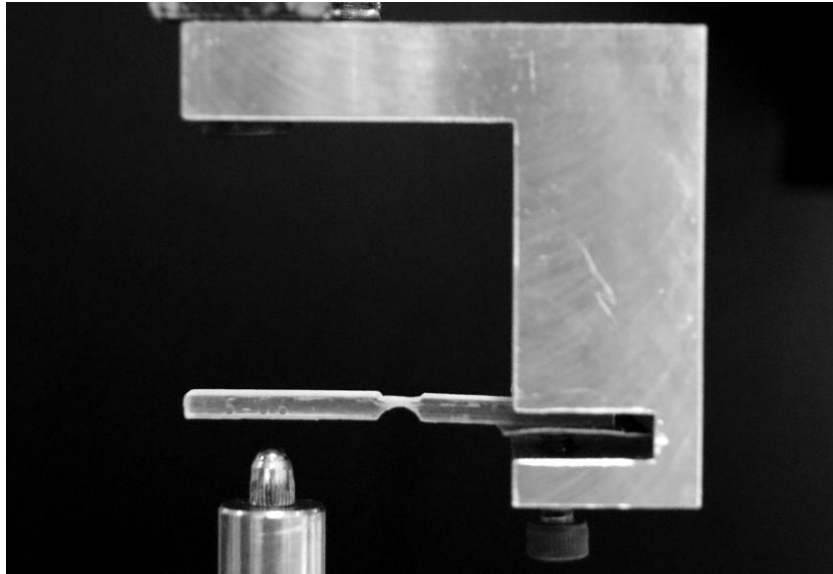


Figure 6.6: Clamp and specimen

Even though the tensile micro-testing machine was not capable of achieving 180 degrees of rotation through circular motion, it was able to achieve 45 degrees bending as shown in Fig 6.7 and accurately measure the force vs vertical displacement.

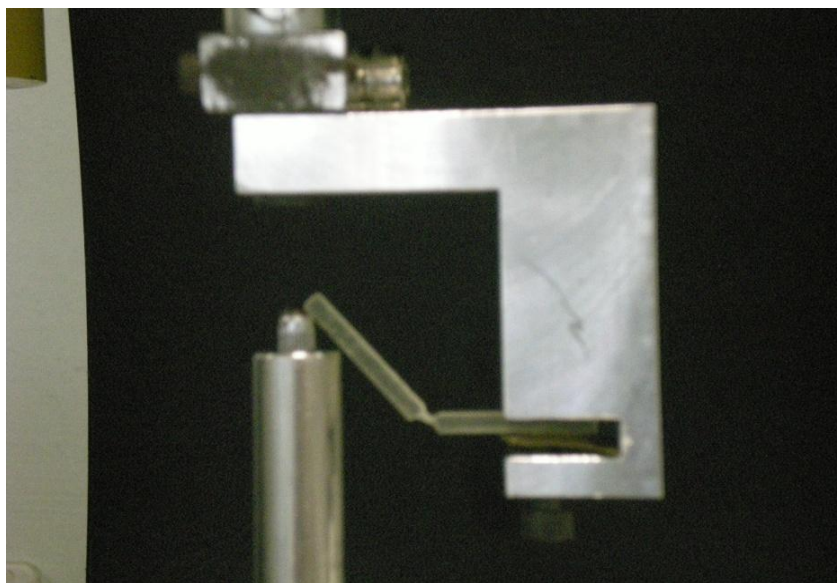


Figure 6.7: 45 degrees bending achieved using the tensile micro-tester

## Chapter 7. Refined Numerical Analysis

The primary objective of this part of the study was to refine the FE model developed in Chapter 5 and adapt it to boundary conditions described in Chapter 6. Since the feature modeled had a constant geometry through-out the cross-section, a two-dimensional model was also developed in order to reduce the solver time.

### 7.2 Refinement of Boundary Conditions

The boundary conditions were defined to closely resemble the boundary conditions of the experimental set-up. The right-hand side of the living hinge was constrained so that it could neither move in the x and y direction nor rotate about the z axis (referred to as ZASYMM constraint in ABAQUS) to replicate the clamping mechanism used in the experiment where a screw pressed on the feature to prevent it from moving. A rigid analytical body was used to model the load pin which was made out of steel as the stiffness of steel is much higher than that of FullCure 720. The rigid body was constrained in the directions except translation along the y axis. As the load pin moved up along the y axis it pushed the feature thus bending it. Figure 7.1 shows the boundary conditions in the experimental set-up while Fig 7.2 depicts the boundary conditions established in the FE model.

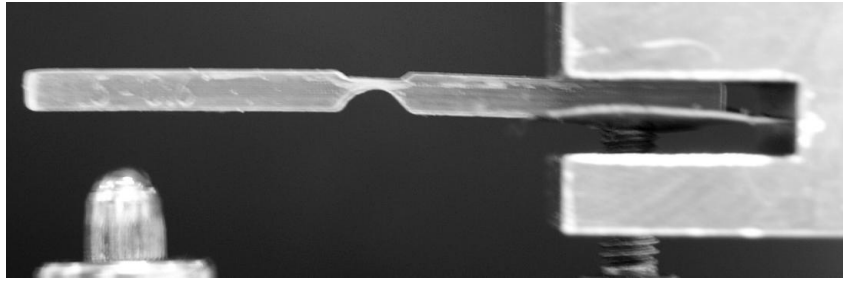


Figure 7.1: Boundary conditions during the experiment

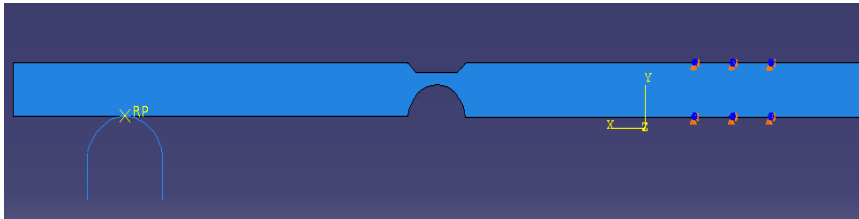


Figure 7.2: Boundary conditions in the FE model

Consequently a three-dimensional model was developed with 5796 eight-noded linear brick, hybrid elements (referred to as C3D8H in Abaqus). The mesh was well refined near the region where the bending takes place with 75 nodes over a 3 mm region. The contact between the load-pin and the specimen was modeled using a penalty friction formulation with a frictional coefficient of 0.2. Fig 7.3 shows a screenshot of the refined model.

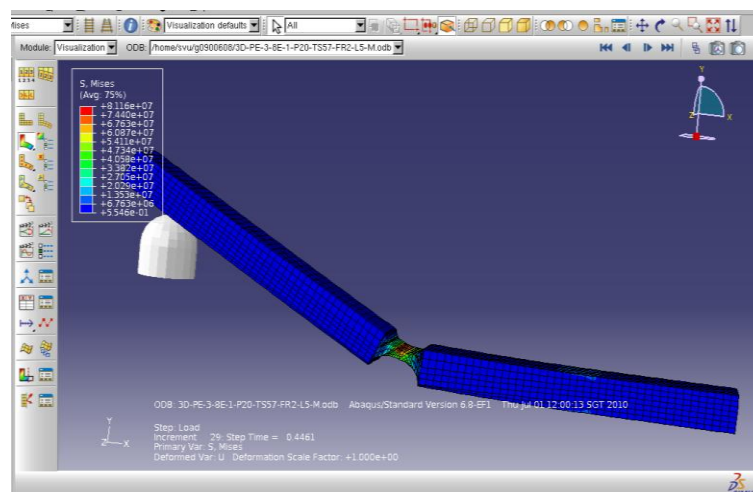


Figure 7.3: Screenshot of the refined FE model



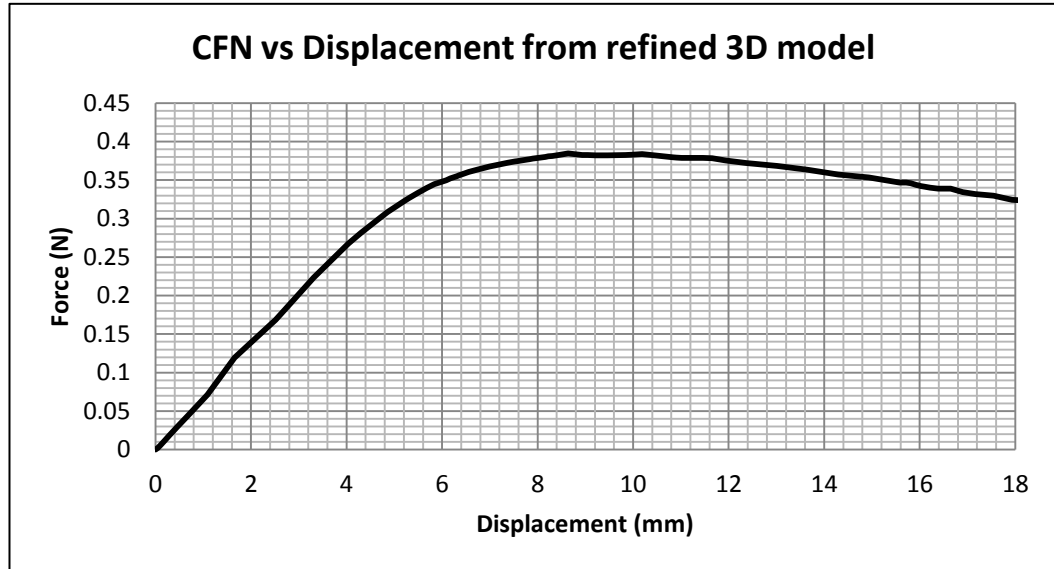


Figure 7.4: CFN vs Displacement from refined 3D model

The output variable CFN signifying the total force due to contact pressure in ABAQUS was used to get results from the simulations. Fig 7.4 shows the result obtained for the specimen of thickness 0.37 mm. There is a decrease in the force once it has attained a peak value which could be attributed to the yielding and the resulting softening of the material. It could also be due to geometrical softening occurring due to necking in the hinge region. Simulations were carried out for living hinge specimens of varying thicknesses in order to compare them to the real life specimens fabricated.

## 7.2 2D Model

Since the feature modeled has a constant geometry through-out the cross-section, a two-dimensional model was tried out in order to reduce the solver time. Simulations were carried for both plane stress (referred to as CPS4 in Abaqus) and plane strain (referred to as CPE4H in Abaqus) elements but the results were not

accurate. While the simulations with the plane stress element type gave the correctly predicted the peak force value, there was excessive local distortion in the neck region which led to unloading in the rest of the feature. On the other hand the simulations with the plane strain element type significantly overestimated the peak force value.

### 7.2.1 Plane stress

Plane stress is defined to be a state of stress in which the normal stress,  $\sigma_z$ , and the shear stresses  $\sigma_{xz}$  and  $\sigma_{yz}$ , directed perpendicular to the x-y plane are assumed to be zero (Bruch). It is commonly used to simplify calculations for continuum structures where one dimension is much smaller than the others and where loads are applied uniformly over the thickness. In the case of a living hinge, the breadth of the specimen was much smaller than the length. As a result, a four nodal quadrilateral plane stress element (CPS4) was used to simulate the functioning of the living hinge. The simulations correctly predicted the peak force value but there was excessive local distortion in the neck region which led to unloading in the rest of the feature once the peak was achieved.

### 7.2.2 Plane strain

Plane strain is defined to be a state of strain in which the strain normal to the x-y plane,  $\epsilon_z$ , and the shear strain  $\gamma_{xz}$  and  $\gamma_{yz}$ , are assumed to be zero (Bruch). It is used to simplify calculations for continuum structures in which the dimension in

one coordinate direction is very large compared to the dimensions in the other 2 directions. The load should be uniformly distributed with respect to the large dimension and act perpendicular to it. In the case of the living hinge, the length of the specimen was much larger than the breadth and the thickness. Consequently, a four nodal bilinear hybrid plane strain element CPE4H was used to simulate the living hinge functioning. While the simulations did not exhibit sudden unloading, they significantly overestimated the peak force value.

It was eventually decided that in order to maintain the accuracy and reliability of the results, all the Finite Element Analysis would be carried using the 3D model.

## **Chapter 8. Experimental verification and application of the numerical model**

The objective of this part of the study was to carry out the experiments proposed and compare the experimental results with the results from the numerical analysis. The numerical results were found to be in line with the experimental results. The numerical model was subsequently used to simulate the functioning of another mechanism which uses elastomeric properties for its functioning: snap fit mechanisms.

### **8.1 Experimental Results**

Experiments were carried out with the experimental setup described in Chapter 6. The force required to displace the hinge specimen was recorded. Multiple experiments were carried out for each dimension of living hinge in order to test the repeatability of the tests. Figure 8.1 and 8.2 show a summary of the experimental results for varying thicknesses and angles of bending (Refer to Appendix C for details). As expected, the force required to bend the hinge increases with the thickness of the neck region. Also, there is a decrease in the force once it has attained a peak value which could be attributed to the yielding and the resulting softening of the material. It could also be due to geometrical softening due to necking in the hinge region.

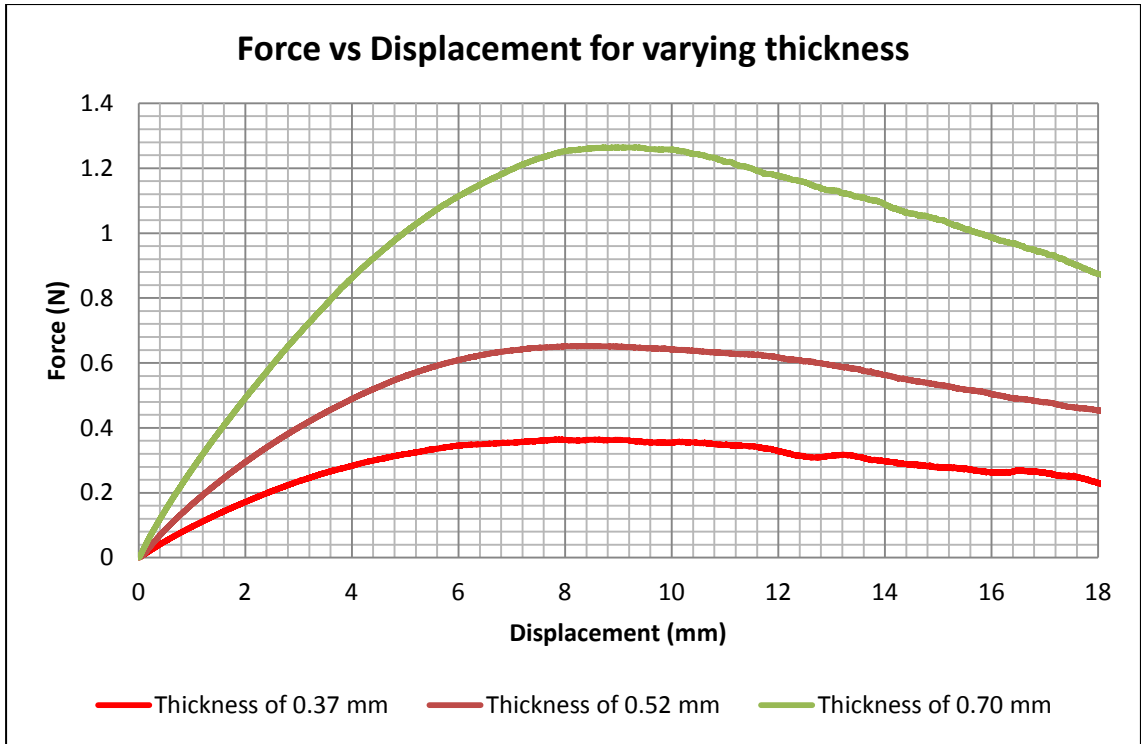


Figure 8.1: Force vs displacment for varying thicknesses

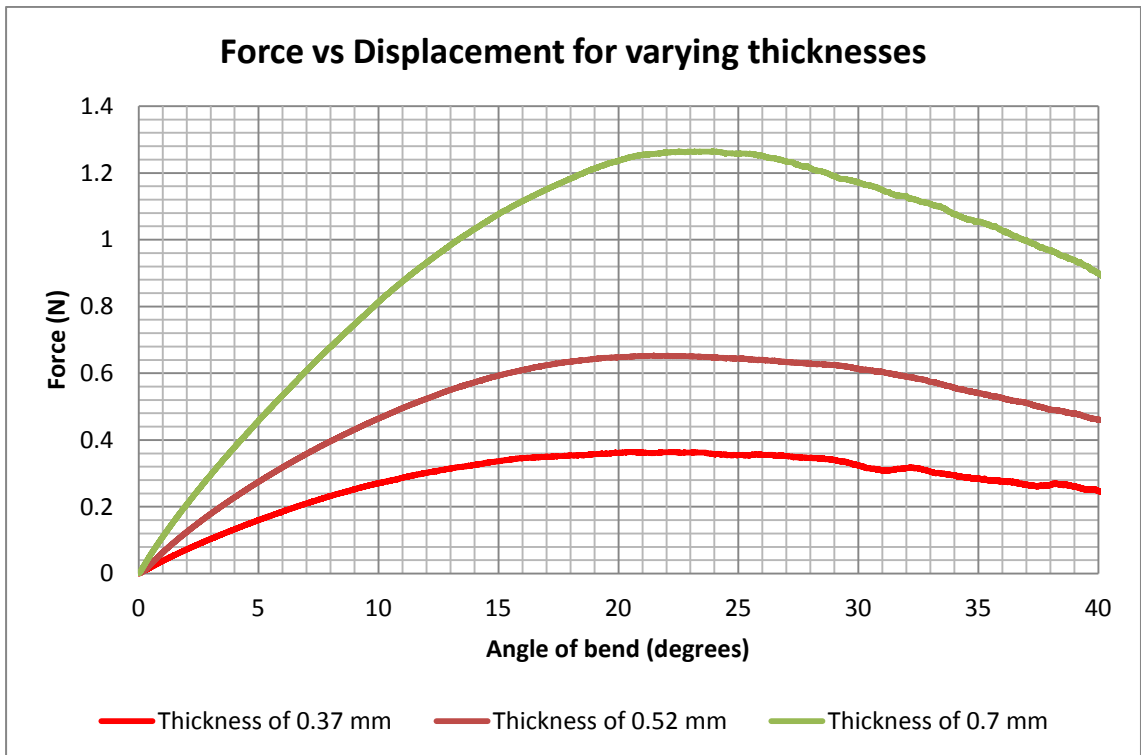


Figure 8.2: Force vs Angle of bend for varying thicknesses

## 8.2 Comparison of Experimental and Numerical results

The results obtained from the experiments were compared against the finite element analyses using the output variable CFN signifying the total force due to contact pressure in Abaqus. Figure 8.3 and 8.4 show the comparison between the specimens of average thickness 0.37 mm and the corresponding FE results while Figure 8.5 and 8.6 show the comparison between the specimens of average thickness 0.70 mm and the corresponding FE results (Refer to Appendix C for details). It is noted that while the results agree closely for low strains, there is a slight divergence between the curves for large strains. This may have been due to the piece-wise power law approximation for large strains and also the predomination of non-linear visco-elasticity at higher strains leading to a decreased Young's modulus (Frank, 1998).

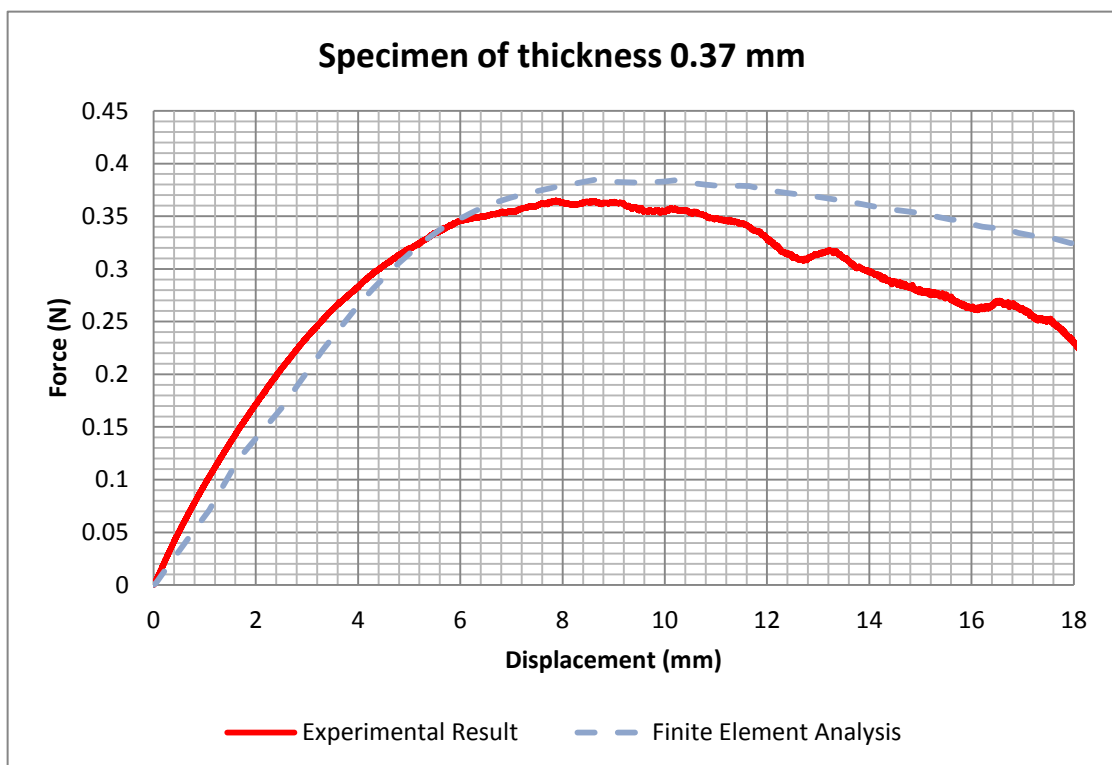


Figure 8.3: Comparison of experimental and numerical analysis for hinge specimen of thickness 0.37mm (displacement)

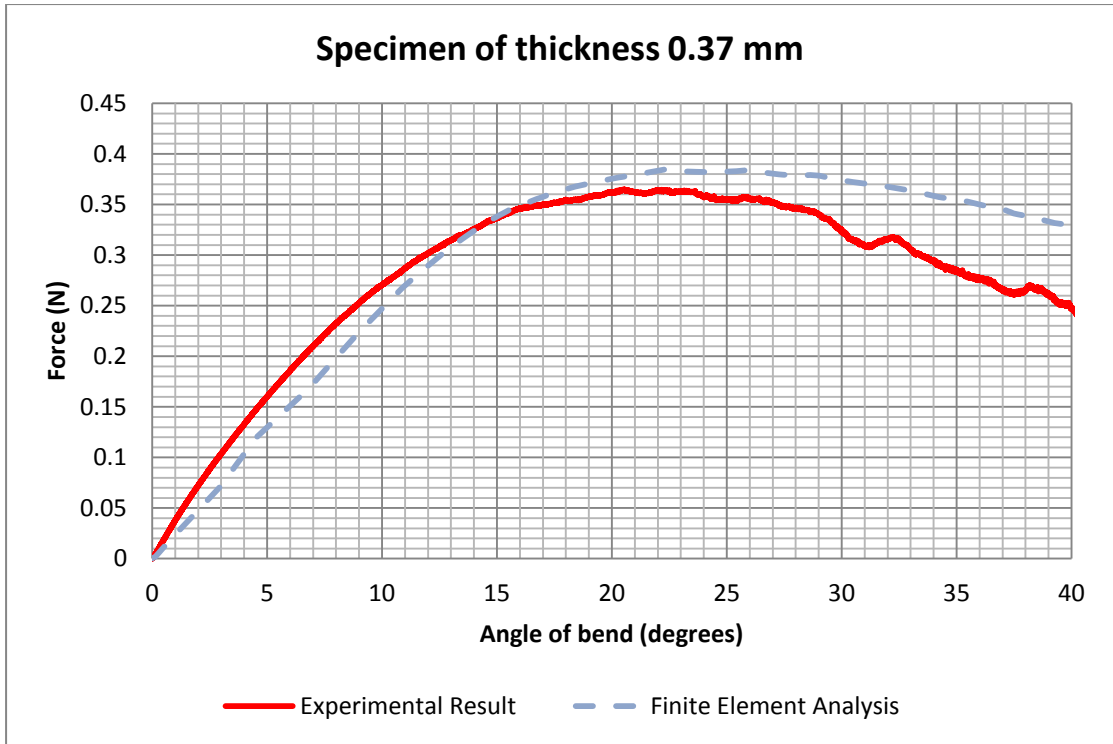


Figure 8.4: Comparison of experimental and numerical analysis for hinge specimen of thickness 0.37mm (degrees)

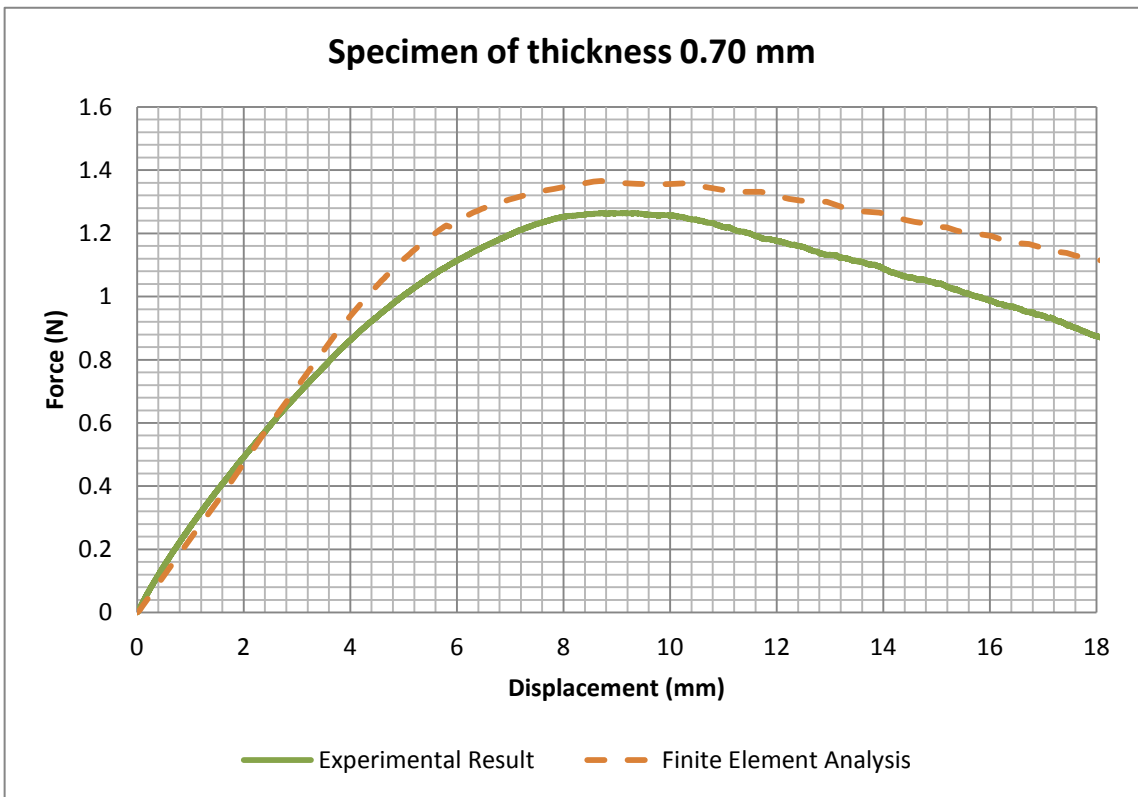


Figure 8.5: Comparison of experimental and numerical analysis for hinge specimen of thickness 0.70mm (displacement)

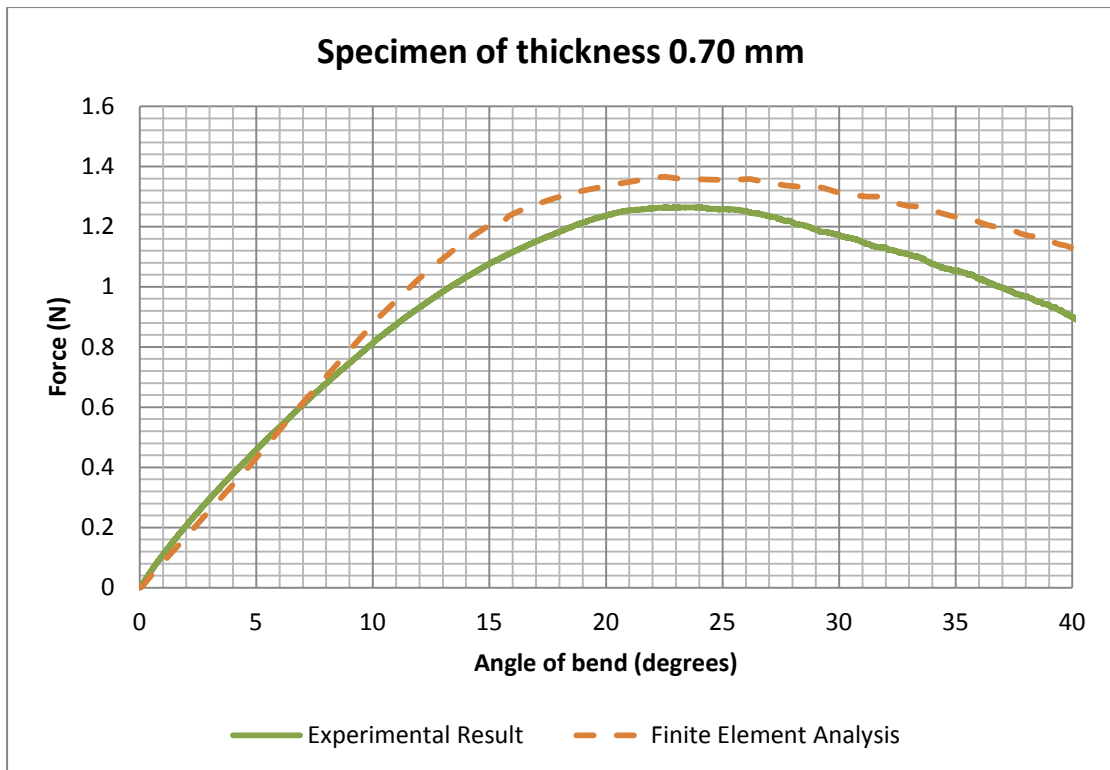


Figure 8.6: Comparison of experimental and numerical analysis for hinge specimen of thickness 0.70mm (degrees)

### 8.3 Application of Numerical Model – Snap Fits

Snap fits are a quick and economical method of joining plastic parts. They reduce assembly costs and are very useful since they reduce the need to have screws, clips, adhesives, etc. Most snap fit designs share the common design features of protruding ledge and a snap foot. This makes the injection mold that produces the parts significantly more complicated and expensive. As a result, snap fits form very good candidates for fabrication using AM. Snap fits ideally require materials which have relatively high elongation, low coefficient of friction and sufficient strength and rigidity. Since FullCure 720 fits these criteria, snap fits were selected to test the numerical model developed earlier for living hinges. There are 3 kinds of snap fit mechanisms (Figure 8.4 and 8.5 show examples of snap fits):



1. Annular snap fits
2. Cantilever snap fits
3. Torsion snap fits

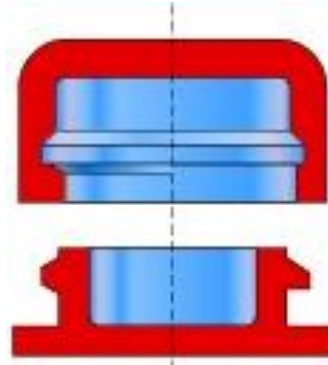


Figure 8.7: Bottle cap - example of an annular snap fit (Source: Core77)

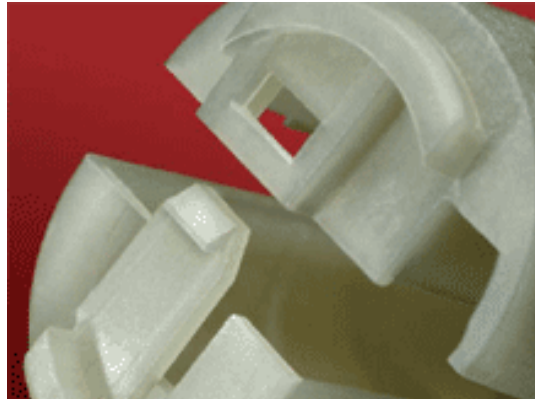


Figure 8.8: Electrical box - example of cantilever snap fit (Source: IDES)

Cantilever snap fits were chosen for this study since they are the most widely used type of snap fit. A hook attached to a cantilever beam is deflected as it is inserted into a hole or past a latch plate. As the hook passes the edge of the hole, the cantilever beam returns to its original shape. The beam could be tapered from the tip to the base to distribute the stress more evenly along the length of the beam (Manner, 2010).

### 8.3.1 Theoretical Modeling of snap-fit mechanisms

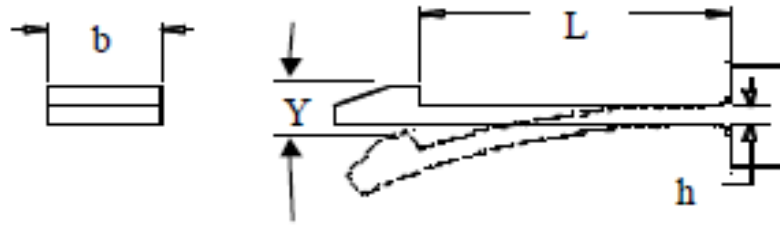


Figure 8.9: Cantilever snap fit

For simplicity, the beam has been assumed to be straight in this study. From beam theory, the maximum stress on the beam is given by:

$$\sigma = \frac{FL}{Z} \quad (8.1)$$

where the section modulus is:

$$Z = \frac{2I}{h} \quad (8.2)$$

and the moment of inertia is:

$$I = \frac{bh^3}{12} \quad (8.3)$$

From Hooke's Law, the relationship between stress and strain is known as:

$$\sigma = E\varepsilon \quad (8.4)$$

Therefore from (8.1), (8.2), (8.3) and (8.4), the force required to deflect the beam:

$$F = \frac{bh^3}{6} \times \frac{E\varepsilon}{L} \quad (8.5)$$

Also from beam theory, the displacement of the beam is given by:

$$Y = \frac{FL^3}{3EI} \quad (8.4)$$

Therefore from (8.4) and (8.5), the strain in the beam is:

$$\varepsilon = \frac{3Yh}{2L^2} \quad (8.4)$$

Assuming that the height of the latch is 1 mm, the beam would have to deflect by 1mm to go past it. Therefore the beam maximum beam deflection Y is 1 mm. The dimensions of the snap fit are assumed to be the following:

Dimensions of the cantilever snap fit	
Beam height (h)	2 mm
Beam length (L)	12 mm
Beam width (b)	5 mm
Young's modulus (E) of FullCure 720	1.7 GPa

Table 8.1: Dimensions of snap fit

Replacing the values in the equations, the force required to deflect the beam is:

$$F = 9.44 \text{ N}$$

The maximum strain in the beam during one cycle is:

$$\varepsilon = 0.02$$

### 8.3.2 Application of numerical model for modeling of snap-fit mechanisms

The numerical model developed using the Drucker Pragar model for FullCure 720 was used to simulate the functioning of snap fits. The initial conditions of the model were adapted for the snap fit design. However, the modeling of the material properties of FullCure 720 was kept unchanged. The displacement boundary condition was used as in the case of living hinges. Figures 8.7 to 8.9 show snapshots of simulation of the snap model functioning using the numerical model earlier developed.

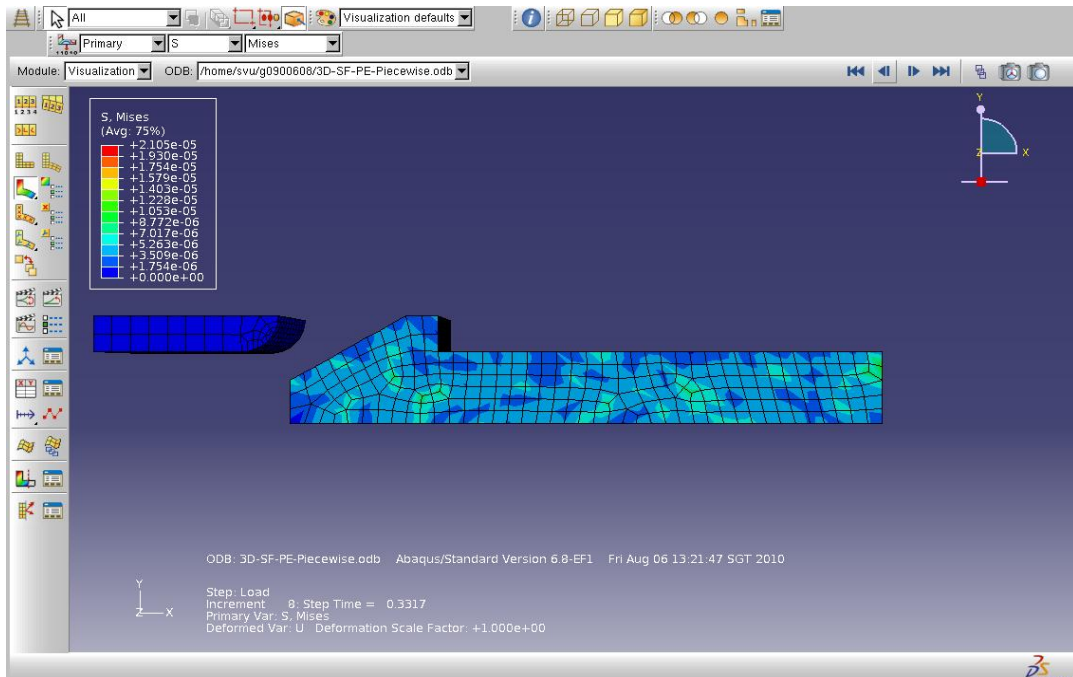


Figure 8.10: Initial position of the snap fit

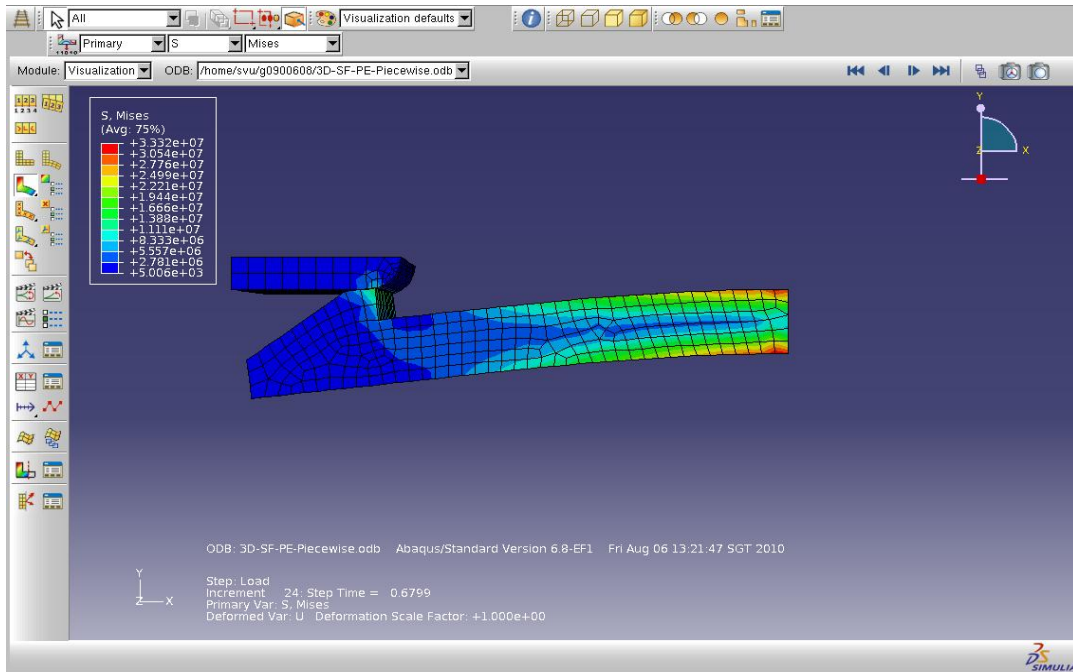


Figure 8.11: Snap fit during deflection

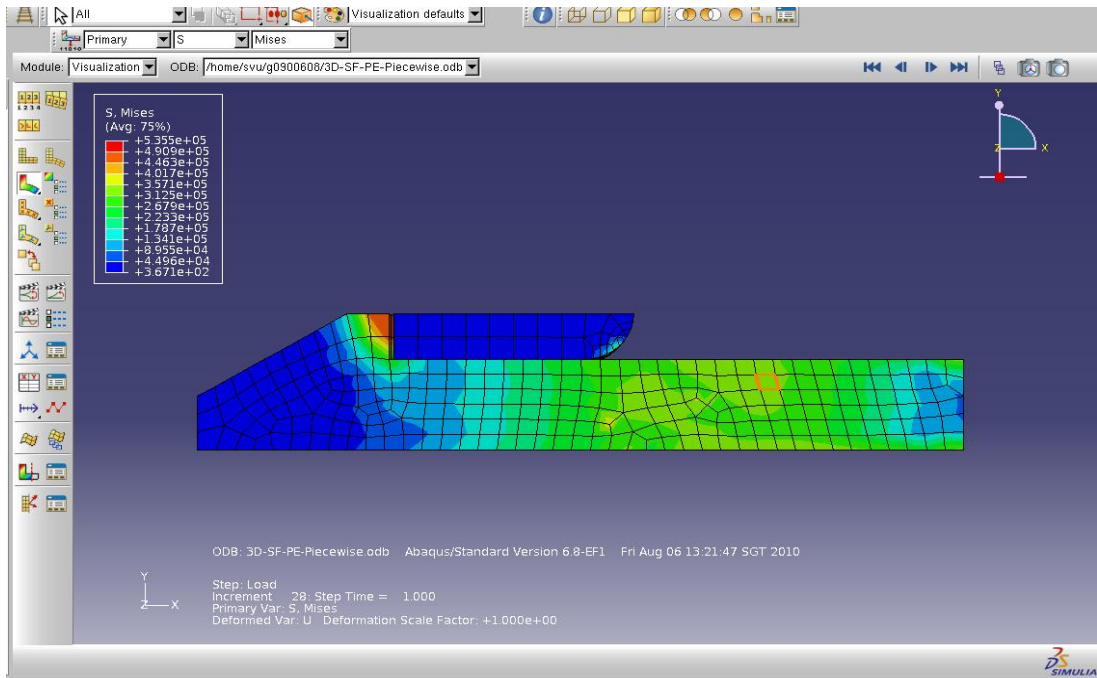


Figure 8.12: Snap fit after passing through ledge

As with the example of living hinges, the output variable CFN was used to estimate the maximum force required to deflect the beam. The force required was found to be 9.87 N. Figure 8.10 shows the reaction force estimated by the model during one cycle. The initial oscillations could have been caused due to the contact between the sharp edge of the hook and the ledge. It was noted that the numerical model provided a similar result as the theoretical model with a variation of 4.5%.

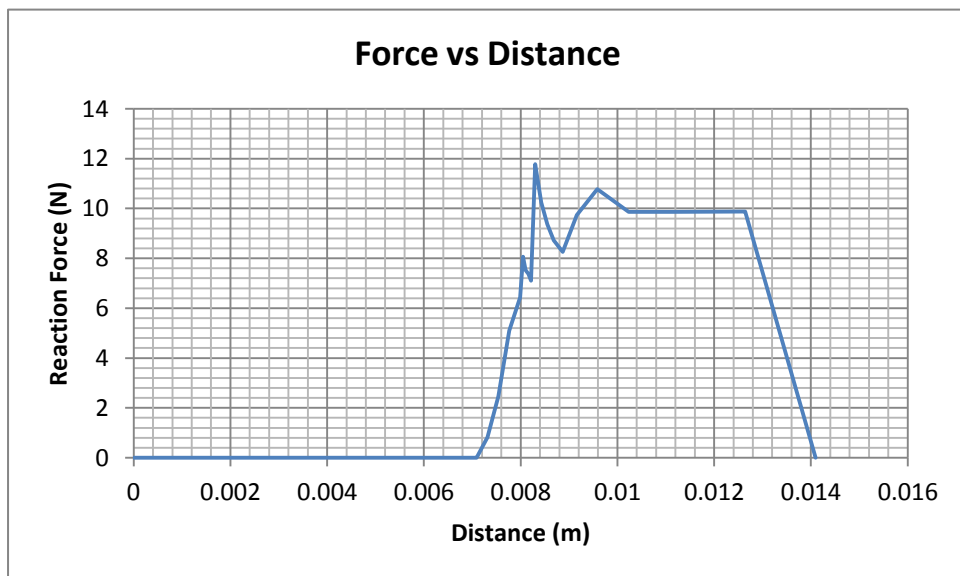


Figure 8.13: Force required to deflect the beam

The output variable Logarithmic Strain – Maximum Principal was used at the point on the right side of the beam which undergoes the highest strain to estimate the maximum strain in the snap fit. The strain was found to be 0.19. Figure 8.11 shows the strain at the point during one cycle. It was noted that the numerical model provided a similar result as the theoretical model with a variation of 5%.

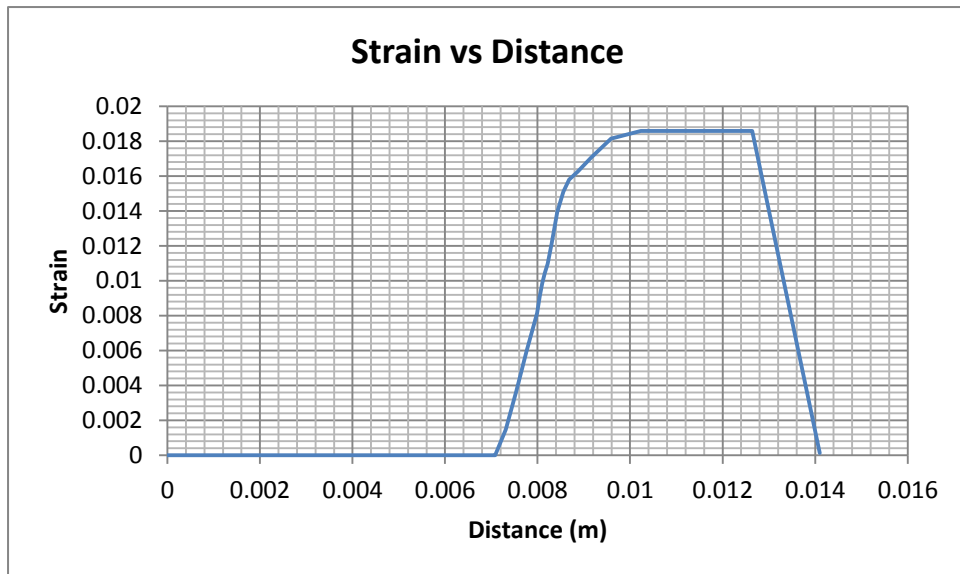


Figure 8.14: Strain on the beam during one cycle

## Chapter 9. Conclusion

This project started out as an investigation into the viability of various AM processes and materials for the fabrication of mechanisms and interlinking structures such as living hinges. Initial analysis led to the hypothesis that it was possible to develop a set of quantifiable rules for living hinges that would allow designers to select the correct process and material from what is available.

A theoretical model based on material indices was developed to aid material and process selection for living hinges through a study of the elastomeric properties of AM materials and the kinematics of the bending mechanism. The initial analysis predicted that FullCure 720 would be a good candidate for the fabrication of living hinges. However preliminary experimental results and a more detailed theoretical study proved otherwise. While FullCure 720 does exhibit elastomeric properties, it is not strong enough to withstand heavy use.

The initial hypothesis thus led to a modified one that states it was possible to develop numerical models using Finite-Element Analysis (FEA) which would be able to predict feature behavior for AM parts. Experiments were carried out to find out the material properties of specimens of FullCure 720 fabricated with Objet Eden 350. The results of the experiments were useful to select the FEA model would be most accurate to simulate the behavior of FullCure 720. Since the compressive yield stress for FullCure 720 was noted to be 1.4 times higher than the tensile yield stress

indicating pressure-sensitive yielding, it was not possible to simulate the test using von Mises plasticity. After studying different plasticity models, the original linear Drucker Prager (DP) model was used in conjunction to the linear elastic model to model the behavior of FullCure 720.

A general FEA model taking living hinges as an example was developed which could be used to model different features that make use of the elastomeric properties of FullCure 720 or similar materials. The study investigated the high deformation which occurs during the bending of a feature and examined the ability of FEA to predict the feature behavior by obtaining simulation results from a model that undergoes high element distortion. The analysis included the modeling of the geometry and boundary conditions, the material properties obtained from the compression tests and structured mesh elements to calculate the contact forces.

An experimental set-up was developed that would closely resemble the real life functioning of a living hinge while allowing repeatability and measurability. The experimental results were compared with the results from the numerical analysis. The FEA model developed appeared to closely approximate and correlate with the experimental results. The model was subsequently used to simulate the functioning of another mechanism which uses elastomeric properties for its functioning: snap fit mechanisms. The numerical results were in-line with expectations proving that the model could potentially be used to understand the functioning of different mechanisms which use elastomeric properties of FullCure 720 for their functioning.



Further studies in the subject could investigate other AM materials and processes. More applications of FullCure 720 itself could also be studied. Sensitivity analysis could be carried out on the FEA model developed to study how the dimensions (especially neck thickness,  $2t$ ) of the living hinge affect the performance of the hinge. This analysis could be helpful for future design of the living hinge. In the case of living hinges, the design-process related properties such as speed of process and part finishing were not very important and thus were not considered in detail. However, for mechanisms such as gears the accuracy and surface finishing of the process might be important and would have to be considered.

In order to better understand the behavior of living hinges itself, a torsion test which could replicate the circular bending of living hinges (described in this study) could be carried out if a sensitive enough torsion machine is available. The numerical model could include the unloading phase of the living hinge which involves the visco-elastic phase. The modeling of material softening as well as crack propagation and fatigue could lead to better prediction of failure.

## Bibliography

Gibson I., Rosen D. W., Stucker B. (2010). Additive Manufacturing Technologies. Springer, 2010.

Bourell D.L., Beaman J.J., Leu M.C., Rosen D.W. (2009). A Brief History of Additive Manufacturing and the 2009 Roadmap for Additive Manufacturing: Looking Back and Looking Ahead. US-Turkey Workshop on Rapid Technologies.

Shankland S, CNET News, (Website: [http://news.cnet.com/8301-30685\\_3-10436841-264.html](http://news.cnet.com/8301-30685_3-10436841-264.html). Retrieved: 6th October, 2010).

Hague R., Mansour S., Saleh N. (2004). Material and design considerations for Rapid Manufacturing. International Journal of Product Research.

Griffiths A. (2002). Rapid Manufacturing, the next industrial revolution. Journal of Materials World.

Pham D.T., Dimov S.S. (2001), Rapid Manufacturing: The Technologies and Applications of Rapid Prototyping and Rapid Tooling, Springer

Sippel, D. (2008), Investigation of detail resolution on basic shapes and development of design rules, EOS

Mansour S., Hague R. (2003). Impact of rapid manufacturing on design for manufacture for injection mouldng. Proceedings of Institution of Mechanical Engineers.

Gibson I., Goenka G., Narasimhan R., Bhat N. (2010). Design Rules for Additive Manufacture. International Solid Freeform Fabrication Symposium.

Yuan L. (2008). A preliminary research on development of a fiber-composite, curved FDM system. Thesis for Master of Engineering, NUS.

Smiley G. (2008) Chapter 6: Rapid Prototyping Processes, Rapid Prototyping and Engineering Applications: A Toolbox for Prototype Development.

Cheung S.H., Choi H.H. (2008). A versatile virtual prototyping system for rapid product development. Computers in Industry, 2008, Vol. 59.

Shapeways. [Online] [Cited: July 7, 2010.] [www.shapeways.com](http://www.shapeways.com).

Freedom of Creation. [Online] [Cited: July 7, 2010.] [www.freedomofcreation.com](http://www.freedomofcreation.com).

MGX. [Online] [Cited: July 7, 2010.] [www.materialise.com/MGX](http://www.materialise.com/MGX).

Hague R., Campbell I., Dickens P. (2003). Implications on Design of rapid manufacturing. *Journal of Mechanical Engineering Science*.

González N, Kerl F. (2008). Design study: living hinges, EOS.

Palli G. (2009) Integrated Mechatronic Design for a New Generation of Robotic Hands.

FullCure 720 Transparent Materials. Objet Geometries . [Online] [Cited: July 8, 2010.] [http://www.objet.com/Materials/FullCure720\\_Transparent/](http://www.objet.com/Materials/FullCure720_Transparent/).

Objet Eden 350/350V. Objet Geometries . [Online] [Cited: July 8, 2010.] [http://www.objet.com/Docs/E350\\_3D%20Printers\\_A4\\_com.pdf](http://www.objet.com/Docs/E350_3D%20Printers_A4_com.pdf)

Pilipovic A., Raos P., Šercer M. (2007). Experimental analysis of properties of materials for rapid prototyping. Springer.

Elleithy R.H. (2007). Plastic Integral Hinges: Design, Processing, and Failure Analysis. Ohio, Society of Plastics Engineers, 2007 .

Vesenjak M., Ochsner A, Ren Z. Computational Modelling of Closed- and Open-Cell Cellular Structures with Fillers.

Abaqus 6.8 Documentation.

Benabdallah H.S. (2006). Static friction coefficient of some plastics against steel and aluminum under different contact conditions. Tribology International, Elsevier.

Geoffrey F.J., Brockman R.A. (1998) A viscoelastic-viscoplastic constitutive model for glass polymers. International Journal of Solids and Structures.

Ashby M.F. (2005). Materials Selection in Mechanical Design.

Gershenfeld N. FAB: The Coming Revolution on Your Desktop--From Personal Computers to Personal Fabrication.

Hill, R. (1967). The mathematical theory of plasticity, OUP, Oxford.

Rabinowitz S., Ward I.M., Parry J.S.C. (1970). The Effect of Hydrostatic Pressure on the Shear Yield Behaviour of Polymers. *Journal of Material Science* 5. pp. 29-39.

Bardia P, Narasimhan R. (2006). Characterization of pressure sensitive yielding in polymers. *Strain* 42. pp. 187-196.

Rabinowitz S., Breadmore P. (1974). Cyclic deformation and fracture of polymers. *Journal of Material Science* 9. pp. 81-99.

Bowden P.B., Jukes J.A. (1972). The plastic flow of isotropic polymers. *Journal of Materials Science* 7. pp. 52-63.

Bauwens J.C.(1970). Yield Condition and Propagation of Luders' Lines in Tension-Torsion Experiments on Polyvinyl Chloride. *Journal of Polymer Science: Part A-2* 8. pp. 893-901.

Du Bois P.A., Kollong S., Frank M. T. (2005). Material behavior of polymers under impact loading. *International Journal of Impact Engineering*.

Drucker, D. C., and Prager W. (1952), Soil Mechanics and Plastic Analysis or Limit Design, *Quarterly of Applied Mathematics*, vol. 10, pp. 157–165.

Bruch Jr, J., Module for Plane Stress and Plane Strain, University of California, Santa-Barbara.

College of Engineering, University of Wisconsin [Online] [Cited: December 30, 2010] <http://homepages.cae.wisc.edu/~me349/>

## Appendix A – Comparison of AM materials for M<sub>1</sub> and M<sub>2</sub>

<b>Process - Injection Moulding</b>		
<b>Material</b>	<b>M1</b>	<b>M2 (MPa)</b>
Polyethylenes	0.038	1.700
Polypropylene	0.030	1.750

<b>Process – Laser sintering of powders (3D Systems)</b>		
<b>Material</b>	<b>M1</b>	<b>M2 (MPa)</b>
Duraform	0.009	0.309
Castform	0.002	0.005
EX	0.032	1.519
Flex	0.243	0.438
Infiltrated Flex	0.250	0.575
GF	0.006	0.166
HST	0.009	0.438
FR 100	0.017	0.545
PA	0.027	1.166

<b>Process - SLA 3D Systems</b>		
<b>Material</b>	<b>M1</b>	<b>M2 (MPa)</b>
Accura Bluestone	0.007	0.465
Accura Xtreme	0.022	0.892
Accura 10	0.021	1.447
Accura 25	0.013	0.499
Accura 40	0.020	1.170
Accura 45HC	0.021	1.259
Accura 48HTR	0.019	1.266
Accura 50	0.019	0.929
Accura 55	0.020	1.304
Accura 60	0.022	1.371
Accura Amethyst	0.008	0.240
Accura Estone	0.023	0.889

<b>Process – Laser sintering of powders (EOS)</b>		
<b>Material</b>	<b>M1</b>	<b>M2 (MPa)</b>
PA2201	0.028	1.355
PA2210	0.018	0.810
PA3200	0.016	0.813



<b>Process - PolyJet Objet</b>		
<b>Material</b>	<b>M1</b>	<b>M2 (MPa)</b>
FullCure830	0.020	0.994
FullCure840	0.020	1.108
FullCure870	0.023	1.173
FullCure720	0.021	1.267
FullCure430	0.019	0.399
FullCure850	0.020	1.200
DM_8510	0.021	1.022
DM_8520	0.020	0.900
DM_8530	0.022	0.869

<b>Process - FDM Stratasys</b>		
<b>Material</b>	<b>M1</b>	<b>M2 (MPa)</b>
ABS	0.014	0.297
ABSi	0.019	0.715
ABSplus	0.016	0.572
ABS/PC	0.019	0.663

## Appendix B – Living hinge specimen dimensions

Expected values are the dimensions specified in the CAD design which was used to fabricate the specimens. There are large differences between the expected dimensions and the dimensions fabricated by the machine, possibly due to calibration errors in the machine. However since the variations between the specimens themselves were very small, the large difference between the expected values and the actual values did not impact the experimental procedures.

<b>Living Hinge 3 - 0.6</b>				
	<b>Length</b>	<b>Thickness</b>	<b>Neck region thickness</b>	<b>Breadth</b>
<b>Expected</b>	<b>45.00</b>	<b>2.50</b>	<b>0.60</b>	<b>4.00</b>
<b>1</b>	45.02	2.29	0.30	3.70
<b>2</b>	45.00	2.27	0.38	3.70
<b>3</b>	45.04	2.31	0.38	3.72
<b>4</b>	45.03	2.33	0.41	3.71
<b>Average</b>	<b>45.02</b>	<b>2.30</b>	<b>0.37</b>	<b>3.71</b>
<b>Standard Deviation</b>	<b>0.017</b>	<b>0.026</b>	<b>0.047</b>	<b>0.010</b>

<b>Living Hinge 3 - 0.8</b>				
	<b>Length</b>	<b>Thickness</b>	<b>Neck region thickness</b>	<b>Breadth</b>
<b>Expected</b>	<b>45.00</b>	<b>2.50</b>	<b>0.80</b>	<b>4.00</b>
<b>1</b>	44.98	2.29	0.57	3.71
<b>2</b>	44.98	2.26	0.48	3.70
<b>3</b>	44.96	2.28	0.53	3.70
<b>4</b>	45.00	2.25	0.50	3.70
<b>Average</b>	<b>44.98</b>	<b>2.27</b>	<b>0.52</b>	<b>3.70</b>
<b>Standard Deviation</b>	<b>0.016</b>	<b>0.018</b>	<b>0.039</b>	<b>0.005</b>

<b>Living Hinge 3 - 1.0</b>				
	<b>Length</b>	<b>Thickness</b>	<b>Neck region thickness</b>	<b>Breadth</b>
<b>Expected</b>	<b>45.00</b>	<b>2.50</b>	<b>1.00</b>	<b>4.00</b>
<b>1</b>	45.03	2.28	0.68	3.70
<b>2</b>	45.03	2.29	0.72	3.71
<b>Average</b>	<b>45.03</b>	<b>2.29</b>	<b>0.70</b>	<b>3.71</b>
<b>Standard Deviation</b>	<b>0.000</b>	<b>0.007</b>	<b>0.028</b>	<b>0.007</b>

## Appendix C – Living hinge experimental results

Summary of experimental results for specimen of thickness 0.37mm (1 in 500 points):

Specimen 1		Specimen 2		Specimen 3		Average	
Load	Extension	Load	Extension	Load	Extension	Load	Extension
N	mm	N	mm	N	mm	N	mm
0.00	0.00	0.00	0.00	0.00	0.00	0.00	0.00
0.03	0.27	0.04	0.27	0.03	0.27	0.03	0.27
0.07	0.67	0.09	0.67	0.08	0.67	0.08	0.67
0.09	0.93	0.12	0.93	0.11	0.93	0.11	0.93
0.12	1.33	0.16	1.33	0.15	1.33	0.15	1.33
0.14	1.60	0.19	1.60	0.18	1.60	0.17	1.60
0.17	2.00	0.23	2.00	0.21	2.00	0.20	2.00
0.19	2.27	0.26	2.27	0.23	2.27	0.23	2.27
0.22	2.67	0.29	2.67	0.26	2.67	0.26	2.67
0.23	2.93	0.31	2.93	0.28	2.93	0.28	2.93
0.25	3.33	0.35	3.33	0.31	3.33	0.30	3.33
0.27	3.60	0.36	3.60	0.33	3.60	0.32	3.60
0.28	4.00	0.39	4.00	0.35	4.00	0.34	4.00
0.29	4.27	0.40	4.27	0.36	4.27	0.35	4.27
0.31	4.67	0.42	4.67	0.38	4.67	0.37	4.67
0.32	4.93	0.44	4.93	0.39	4.93	0.38	4.93
0.33	5.33	0.45	5.33	0.41	5.33	0.39	5.33
0.34	5.60	0.46	5.60	0.41	5.60	0.40	5.60
0.35	6.00	0.47	6.00	0.42	6.00	0.41	6.00
0.35	6.27	0.48	6.27	0.43	6.27	0.42	6.27
0.35	6.67	0.48	6.67	0.43	6.67	0.42	6.67
0.35	6.93	0.49	6.93	0.44	6.93	0.43	6.93
0.36	7.33	0.49	7.33	0.44	7.33	0.43	7.33
0.36	7.60	0.49	7.60	0.44	7.60	0.43	7.60
0.36	8.00	0.50	8.00	0.44	8.00	0.43	8.00
0.36	8.27	0.50	8.27	0.44	8.27	0.43	8.27
0.36	8.67	0.50	8.67	0.44	8.67	0.43	8.67
0.36	8.93	0.49	8.93	0.44	8.93	0.43	8.93
0.36	9.33	0.49	9.33	0.44	9.33	0.43	9.33
0.35	9.60	0.49	9.60	0.44	9.60	0.43	9.60
0.35	10.00	0.48	10.00	0.44	10.00	0.43	10.00
0.36	10.27	0.48	10.27	0.44	10.27	0.42	10.27
0.35	10.67	0.47	10.67	0.43	10.67	0.42	10.67
0.35	10.93	0.46	10.93	0.43	10.93	0.41	10.93
0.34	11.33	0.46	11.33	0.43	11.33	0.41	11.33
0.34	11.60	0.45	11.60	0.42	11.60	0.41	11.60
0.33	12.00	0.45	12.00	0.42	12.00	0.40	12.00
0.32	12.27	0.44	12.27	0.41	12.27	0.39	12.27
0.31	12.67	0.43	12.67	0.41	12.67	0.38	12.67

Specimen 1		Specimen 2		Specimen 3		Average	
Load	Extension	Load	Extension	Load	Extension	Load	Extension
N	mm	N	mm	N	mm	N	mm
0.31	12.93	0.42	12.93	0.40	12.93	0.38	12.93
0.32	13.33	0.41	13.33	0.39	13.33	0.37	13.33
0.31	13.60	0.41	13.60	0.38	13.60	0.37	13.60
0.30	14.00	0.40	14.00	0.37	14.00	0.36	14.00
0.29	14.27	0.40	14.27	0.37	14.27	0.35	14.27
0.29	14.67	0.38	14.67	0.36	14.67	0.34	14.67
0.28	14.93	0.38	14.93	0.35	14.93	0.34	14.93
0.28	15.33	0.37	15.33	0.34	15.33	0.33	15.33
0.27	15.60	0.36	15.60	0.34	15.60	0.32	15.60
0.26	16.00	0.35	16.00	0.33	16.00	0.31	16.00
0.26	16.27	0.33	16.27	0.33	16.27	0.31	16.27
0.27	16.67	0.32	16.67	0.32	16.67	0.30	16.67
0.26	16.93	0.31	16.93	0.31	16.93	0.29	16.93
0.25	17.33	0.31	17.33	0.30	17.33	0.29	17.33
0.25	17.60	0.30	17.60	0.29	17.60	0.28	17.60
0.23	18.00	0.29	18.00	0.29	18.00	0.27	18.00

Summary of experimental results for specimen of thickness 0.70mm (1 in 500 points):

Specimen 1		Specimen 2		Average	
Load	Extension	Load	Extension	Load	Extension
N	mm	N	mm	N	mm
0.00	0.00	0.00	0.00	0.00	0.00
0.09	0.33	0.11	0.33	0.10	0.33
0.18	0.67	0.20	0.67	0.19	0.67
0.25	1.00	0.29	1.00	0.27	1.00
0.32	1.33	0.38	1.33	0.35	1.33
0.39	1.67	0.45	1.67	0.42	1.67
0.45	2.00	0.53	2.00	0.49	2.00
0.51	2.33	0.60	2.33	0.56	2.33
0.58	2.67	0.68	2.67	0.63	2.67
0.63	3.00	0.74	3.00	0.69	3.00
0.69	3.33	0.81	3.33	0.75	3.33
0.75	3.67	0.87	3.67	0.81	3.67
0.80	4.00	0.92	4.00	0.86	4.00
0.85	4.33	0.98	4.33	0.91	4.33
0.89	4.67	1.03	4.67	0.96	4.67
0.93	5.00	1.08	5.00	1.00	5.00
0.97	5.33	1.12	5.33	1.04	5.33
1.01	5.67	1.16	5.67	1.08	5.67
1.04	6.00	1.19	6.00	1.11	6.00
1.06	6.33	1.22	6.33	1.14	6.33
1.09	6.67	1.25	6.67	1.17	6.67

Specimen 1		Specimen 2		Average	
Load	Extension	Load	Extension	Load	Extension
N	mm	N	mm	N	mm
1.11	7.00	1.28	7.00	1.20	7.00
1.13	7.33	1.31	7.33	1.22	7.33
1.14	7.67	1.34	7.67	1.24	7.67
1.15	8.00	1.35	8.00	1.25	8.00
1.16	8.33	1.36	8.33	1.26	8.33
1.16	8.67	1.36	8.67	1.26	8.67
1.16	9.00	1.36	9.00	1.26	9.00
1.17	9.33	1.36	9.33	1.26	9.33
1.16	9.67	1.36	9.67	1.26	9.67
1.17	10.00	1.35	10.00	1.26	10.00
1.16	10.33	1.33	10.33	1.25	10.33
1.15	10.67	1.32	10.67	1.24	10.67
1.14	11.00	1.30	11.00	1.22	11.00
1.12	11.33	1.29	11.33	1.21	11.33
1.10	11.67	1.28	11.67	1.19	11.67
1.09	12.00	1.26	12.00	1.18	12.00
1.08	12.33	1.25	12.33	1.16	12.33
1.06	12.67	1.23	12.67	1.14	12.67
1.05	13.00	1.21	13.00	1.13	13.00
1.03	13.33	1.21	13.33	1.12	13.33
1.01	13.67	1.20	13.67	1.10	13.67
0.99	14.00	1.19	14.00	1.09	14.00
0.95	14.33	1.18	14.33	1.07	14.33
0.94	14.67	1.17	14.67	1.05	14.67
0.93	15.00	1.15	15.00	1.04	15.00
0.92	15.33	1.13	15.33	1.02	15.33
0.90	15.67	1.10	15.67	1.00	15.67
0.88	16.00	1.09	16.00	0.99	16.00
0.87	16.33	1.08	16.33	0.97	16.33
0.85	16.67	1.06	16.67	0.95	16.67
0.84	17.00	1.04	17.00	0.94	17.00
0.83	17.33	1.01	17.33	0.92	17.33
0.82	17.67	0.98	17.67	0.90	17.67